



# Structure-type classification and flexibility-based detection of earthquake-induced damage in full-scale RC buildings

Giacomo Bernagozzi<sup>1</sup> · Said Quqa<sup>1</sup> · Luca Landi<sup>1</sup> · Pier Paolo Diotallevi<sup>1</sup>

Received: 30 December 2021 / Revised: 22 April 2022 / Accepted: 11 May 2022 / Published online: 16 June 2022  
© The Author(s) 2022

## Abstract

Detecting early damage in civil structures is highly desirable. In the area of vibration-based damage detection, modal flexibility (MF)-based methods have proven to be promising tools for promptly identifying changes in the global structural behavior. Many of these methods have been developed for specific types of structures, giving rise to different approaches and damage-sensitive features (DSFs). Although structural type classification is an important part of the damage detection process, this part of the process has received little attention in most literature and often relies on the use of a-priori engineering knowledge. Moreover, in general, experimental validations are only performed on small-scale laboratory structures with controlled artificial damage (e.g., imposed stiffness reductions). This paper proposes data-driven criteria for structure-type classification usable in the framework of MF-based damage identification methods to select the most appropriate algorithms and DSFs for detecting and localizing structural anomalies. This paper also tests the applicability of the proposed classification criteria and the damage identification methods on full-scale reinforced concrete (RC) structures that have experienced earthquake-induced damage. The considered structures are a seven-story RC wall building and a five-story RC frame building, which were both tested on the large-scale University of California, San Diego-Network for Earthquake Engineering Simulation (UCSD-NEES) shaking table.

**Keywords** Structural health monitoring · Earthquake-induced damage detection · Modal flexibility · Wall building · Frame building · Output-only modal identification

## 1 Introduction

Structural health monitoring (SHM) is a fundamental decision support tool to structure and infrastructure managers [1], as it can provide early alerts about potential damage and modifications in the structural behavior, which can guide maintenance and retrofitting interventions. Common vibration-based SHM techniques exploit ambient vibration in an output-only monitoring strategy, thus not involving the knowledge of structural excitation [2, 3]. Among these methods, modal-based approaches are the most used [1]. The recent development of automated modal identification techniques [4] has contributed to closing the gap between the identification of structural parameters and their use in SHM.

In this context, modal flexibility (MF)-based tools have proven to be particularly promising [5–21]. In these methods, identified natural frequencies and mode shapes are used to evaluate an estimate of the structural flexibility matrix, which is an experimentally derived model of the structure. Several damage identification methods rely on displacement estimates obtained by applying virtual loads on the monitored structures (also known as inspection loads), i.e., multiplying the flexibility matrix with a load vector. This way, information contained in the modal flexibility matrix is condensed in a deflection vector, which is considered a synthetic damage-sensitive feature (DSF). Several variants of this general approach were developed in the late '90s [10] and progressively refined over the last few decades [11–21]. Similar approaches for damage localization were also developed to be applied from static deflections [22].

Although all MF-based damage identification methods have some inherent common characteristics, specific features depend upon the type of structures for which the method was developed. Indeed, these methods can be grouped into two

✉ Giacomo Bernagozzi  
giacomo.bernagozzi2@unibo.it

<sup>1</sup> Department DICAM, University of Bologna, Viale del Risorgimento 2, 40136 Bologna, Italy

main classes: methods developed for shear-type structures [11–14] and methods developed for flexure-type structures [15–19]. When considering the damage detection process, being in one category or in the other is relevant for the selection of appropriate inspection loads and for the estimation of appropriate DSFs. Structural type classification is thus an important part of the identification process, required to correctly apply the considered methods. It is worth emphasizing, however, that this part has received little attention in relevant literature and, in most cases, an initial assumption is made about the structural typology, based on the experience of operators. In this framework, it is thus evident that it could be useful to integrate the process by defining data-driven criteria for structural type classification.

MF-based methods for damage detection mentioned in the previous paragraph are briefly reviewed herein. In [11], an approach was proposed for detecting and localizing structural anomalies in buildings that can be modeled as planar shear-type structures. An extension of the mentioned study was presented in [12], where asymmetric damage was considered for plan-symmetric shear-type buildings. In [13], different strategies were presented for damage identification with minimal or no a-priori information about structural masses, even if masses are varied before and after damage. In [15], a steel grid laboratory model was analyzed for damage localization using an MF-based approach. In [16], the concept of Positive Bending Inspection Load (PBIL) was introduced and tested for damage localization in simply supported and continuous beams. In [17], the normalized curvature of the uniform load surface evaluated from modal flexibility was employed for damage localization of numerical models representing cantilever and simply supported beams, considering measured degrees-of-freedom (DOFs) at equal spacing. In [18], the structural responses collected at all stories of a laboratory ten-story frame with constant interstory heights were used to localize damage. In [20], MF-based methods were used for condition assessment in real-life bridges. Moreover, in [21], the approach presented in [11] was validated on a full-scale shear building, where damage was imposed by replacing a spring member with other members having reduced stiffness. Although the last mentioned studies consider full-scale structures, most applications in this field were performed on small-scale laboratory structures.

Based on these premises, the importance of full-scale case studies and applications is evident to assess the effectiveness of MF-based methods for SHM.

This paper has two main objectives: first, propose original data-driven criteria for structure-type classification that, within the framework of the MF-based methods for damage detection, can be useful for selecting the algorithms and the damage-sensitive features that are most appropriate for the considered structure; and second, test the applicability of

the classification criteria and MF-based methods for damage localization on full-scale reinforced concrete (RC) structures that have experienced earthquake-induced damage. The structures considered in this study are a seven-story RC wall building and a five-story RC frame building.

## 2 Damage detection through modal flexibility-based deflections in building structures: an overview

The modal parameters identified during a vibration test can be employed to calculate a modal flexibility matrix, which is an estimate of the static flexibility matrix of the identified system. In input–output tests, the flexibility matrix can be directly extracted from the data if both the input force and the output response are measured for at least one degree of freedom. This requirement guarantees mass normalization of mode shapes. On the other hand, for output-only tests, the modal flexibility matrix is not readily available from the data [8]. However, mass-normalizing constants can be obtained from shape scaling techniques, which generally need the execution of additional tests with some imposed structural modifications [3], a-priori estimates of the system mass matrix [11, 12], or FEM models [3]. Also, proportional mass matrices (PMMs) and flexibility matrices (PFMs), which represent unscaled matrices proportional to the mass and flexibility matrices of the structure, respectively, can be estimated [6, 8, 9, 13, 23]. In this case, a typical assumption to conduct damage identification is that masses are unchanged before and after the damage [6, 13].

The modal flexibility matrix of a generic MDOF system with classical damping can be calculated from modal parameters as [7–9]

$$\mathbf{F}_{r \times n} = \sum_{i=1}^r \frac{1}{(s_i \omega_i)^2} \boldsymbol{\psi}_i \boldsymbol{\psi}_i^T, \quad (1)$$

where  $n$  is the number of DOFs measured on the structure,  $r$  is the number of the modes included in the calculation,  $\boldsymbol{\psi}_i$  is the  $i$ th real and arbitrarily scaled mode shape vector (with dimensions  $n \times 1$ ),  $\omega_i$  is the  $i$ th natural circular frequency, and  $s_i$  is the mass normalization factor of the  $i$ th mode.

Modal flexibility deflections, represented by the vector  $\mathbf{v}_{n \times 1}$ , can thus be determined by applying some inspection loads (collected in the vector  $\mathbf{p}_{n \times 1}$ ) to the flexibility-based model, as follows:

$$\mathbf{v} = \mathbf{F}_r \mathbf{p}. \quad (2)$$

The content of the modal flexibility matrix is thus condensed in the deflection vector.

Depending on the type of structures, different inspection loads should be selected. In the same way, the choice of the specific damage-sensitive features to be extracted from the estimated deflections also depends upon the type of structure. Referring to building structures, considered in this study, two modeling schemes have been mainly considered in the literature to derive the deflection-based approaches for damage identification. On one side, for buildings composed of RC walls, one of the simplest modeling approaches is to consider such structures as bending moment-deflecting cantilever structures (Fig. 1a). On the other side, for RC frame buildings, one of the simplest modeling approaches is to consider such structures as shear-type structures (Fig. 1b), and the more such a model is valid and effective, the more the rigidity of horizontal beams is comparable to (or even higher than) the rigidity of columns.

When considering bending moment-deflecting cantilever structures, a Positive Bending Inspection Load (PBIL) should be selected as the inspection load. This concept was introduced in [16], where the more general case of bending moment-deflecting beam-like structures is studied (considering, for example, simply supported beams or multi-span continuous beams). The work [16] studies planar structures in one direction and shows the relationship between damage in beam-like structures (e.g., localized stiffness reduction) and the damage-induced deflection, i.e., the difference between the deflections in the damaged and undamaged states. The PBIL is defined as a load that generates positive bending moments and no inflection points in a given inspection region of the structure [16]. For a cantilever structure, a convenient inspection load for evaluating the modal flexibility-based deflections is a uniform load with unitary values at all the DOFs—i.e.,

$\mathbf{p} = \{1 \ 1 \ \dots \ 1\}^T$  (Fig. 1a). This load is indeed a PBIL load for a cantilever structure, as shown in [16].

Different features computed from these deflections can be used for damage detection [15–18]. The most well-known approach is to evaluate the curvature of the deflection, as shown in [15, 17]. For damage detection in structures that exhibit bending behavior, the curvature was initially evaluated on the mode shapes [24]. Then, the criterion has been also adopted in the case of the deflections computed from the modal flexibility matrix (also known in the literature as uniform load surface).

The rotations and the curvatures of estimated deflections can be calculated using the finite difference method, as a numerical derivation technique. The rotation of a portion of the structure located between two measured DOFs—i.e., the  $(j+1)$ th and the  $j$ th DOFs—can be calculated as follows:

$$\varphi_{(j+1,j)} = \frac{v_{j+1} - v_j}{H_{j+1} - H_j}, \quad (3)$$

where  $H_j$  is the height of the  $j$ th DOF evaluated with respect to the base of the cantilever structure. If the measured DOFs are located at a constant spacing  $h$ , which is the case of the most common layout of instrumented locations to be adopted in practice, Eq. (3) simplifies as follows:

$$\varphi_{(j+1,j)} = \frac{v_{j+1} - v_j}{h}. \quad (4)$$

Besides, the curvature at the  $j$ th measured DOF of the modal flexibility-based deflections can be estimated as

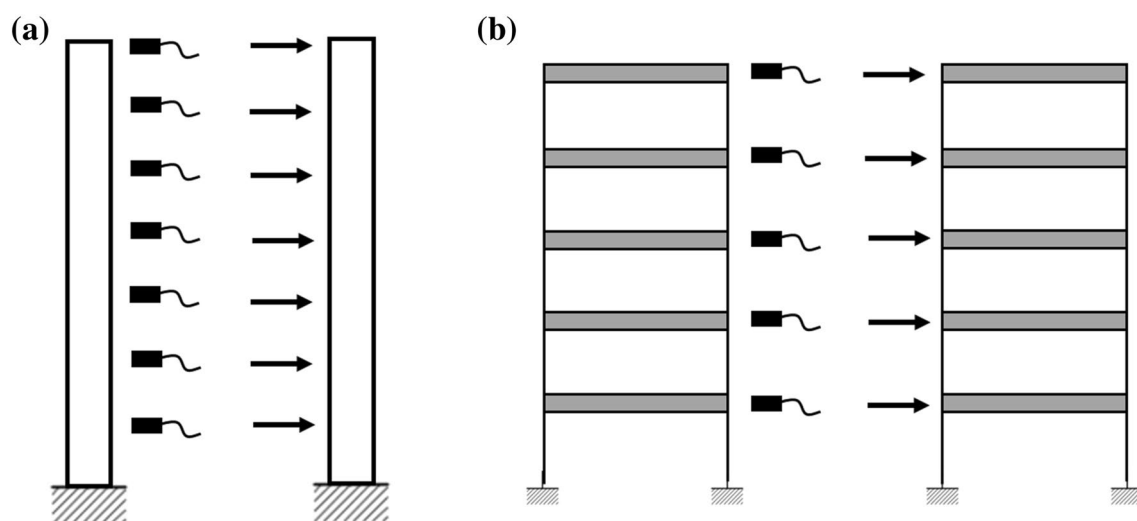


**Fig. 1** Structural models with instrumented locations and applied inspection loads: **a** bending moment-deflecting cantilever structure; **b** shear-type frame structure

$$\chi_j = \frac{\frac{v_{j+1}-v_j}{H_{j+1}-H_j} - \frac{v_j-v_{j-1}}{H_j-H_{j-1}}}{\frac{H_{j+1}-H_{j-1}}{2}}. \quad (5)$$

Equation (5) is also valid for measured DOFs that are unevenly distributed along with the height of the structure. Such an equation was obtained by adapting the formulation presented in [25]. If the measured DOFs are located at a constant spacing equal to  $h$ , Eq. (5) simplifies as follows:

$$\chi_j = \frac{v_{j+1} - 2v_j + v_{j-1}}{h^2}. \quad (6)$$

Of course, uncertainties are always present in the quantities extracted from real noisy vibration data. Thus, statistical approaches based on outlier analysis [1] can be included in the damage localization process to estimate the degree of variability that affects the quantities related to the baseline structure.

According to [17], curvature estimates should be monitored to understand if they deviate from the baseline condition. In this case, structural damage is likely to have occurred. This strategy is implemented by calculating the following index, termed here as  $z$ -index based on curvature:

$$z_{\chi_j} = \frac{\chi_{I,j} - \bar{\chi}_{B,j}}{s(\chi_{B,j})}. \quad (7)$$

Equation (7) can be evaluated for each  $j$ th measured DOF with  $j = 1 \dots n-1$ , where  $j = 1$  is the first measured DOF at the bottom of the structure. In Eq. (7),  $\chi_{I,j}$  is the curvature related to the structure in the inspection stage, while  $\bar{\chi}_{B,j}$  and  $s(\chi_{B,j})$  are the sample mean and the sample standard deviation of the curvature  $\chi_{B,j,i}$  evaluated from a training data set (for  $i = 1 \dots g$  where  $g$  is the total number of damage-sensitive features extracted from the training data set).

Damage can be detected and localized by comparing the calculated  $z$ -index with a threshold value  $z^{\text{TH}}$ . Specifically, for the  $j$ th measured DOF, the structure in the inspection stage can be considered as unaltered with respect to the baseline structure if  $z_{\chi_j} \leq z^{\text{TH}}$ . On the other hand, if  $z_{\chi_j} > z^{\text{TH}}$ , the structure in the inspection stage deviates from the baseline. As shown in [17], it is assumed that the features extracted from the training data set have a normal distribution. Moreover, as also discussed in [17], the value of the threshold is a user choice, to be set for controlling the trade-off between false positives and false negatives. In the present paper, the value of the threshold is assumed as equal to  $z^{\text{TH}} = 3$ , as it is also done in [12, 13] where similar statistical tests have been performed.

For shear-type structures, a Positive Shear Inspection Load (PSIL) should be selected as the inspection load, which is a load that induces positive shear forces in each

story of the structure. This concept was introduced in [11], where planar frame structures, regular in height (both in terms of stiffness and mass), and with constant interstory height, are analyzed in one direction. Among the different PSIL loads, [11] suggests to select a uniform load with unitary values at all the DOFs—i.e.,  $\mathbf{p} = \{1 \ 1 \dots 1\}^T$  (Fig. 1b), which, as described in the previous paragraphs, is the same load considered for bending moment-deflecting cantilever structures. To apply the damage detection method presented in [11], horizontal vibration measurements should be acquired at all the stories of the structure. This does not necessarily imply having a one-to-one correspondence between the stories and the available sensors. For example, in ambient vibration tests, the case of a limited number of available sensors can be addressed using multi-setup output-only identification test and existing approaches for mode shape merging [3]. An example where this strategy is applied in the context of a flexibility deflection-based damage detection process is shown in [12].

Reference [11] also shows that damage in shear-type buildings (e.g., local stiffness reduction) at a certain story generates damage-induced deflections with non-zero interstory drift variation only at that specific story. For shear-type building structures, the interstory drifts are thus assumed as damage-sensitive features, and such quantities can be calculated from the estimated modal flexibility-based deflections as follows:

$$d_j = \begin{cases} v_j - v_{j-1} & \text{for } j = 2 \dots n \\ v_j & \text{for } j = 1. \end{cases} \quad (8)$$

Similar to the previous case of bending moment-deflecting cantilever structures, a statistical approach can be used for localizing damage in shear-type structures [11]. For these structures, the damage index can be evaluated as follows:

$$z_{d_j} = \frac{d_{j,I} - \bar{d}_{j,B}}{s(d_{j,B})}, \quad (9)$$

which is termed herein as  $z$ -index based on interstory drifts and which refers to the  $j$ th story of the building. Equation (9) uses quantities related to both the inspection stage (subscript I) and the baseline state (subscript B). As already shown for Eq. (7), the operators  $\bar{\cdot}$  and  $s(\cdot)$  calculate the sample mean and the sample standard deviation, respectively, and are applied on quantities related to the baseline state.

The statistical test should then be performed. For a shear-type building structure, damage is located at the  $j$ th story if  $z_{d_j} > z^{\text{TH}}$ , where  $z^{\text{TH}}$  is the threshold value. On the other hand, no damage is identified at the  $j$ th story if  $z_{d_j} \leq z^{\text{TH}}$ . According to [11], the same considerations about the threshold value  $z^{\text{TH}}$  already made in the previous paragraphs for the case of the bending moment-deflecting

cantilever structure are also valid for the case of the shear-type building structure. For this last case, this study assumes  $z^{TH} = 3$ .

### 3 Proposed criteria for cantilever structure-type classification

Different criteria are proposed in the following to classify the monitored building structures and to select the appropriate damage detection method—i.e., the methodology developed for bending moment-deflecting cantilever structures based on the estimation of the curvature of the modal flexibility-based deflections or the methodology developed for shear-type building structures based on the evaluation of the interstory drifts. The proposed criteria should be applied using experimentally identified modal parameters, and reference solutions computed from continuous cantilever beam models are used to perform the classification of the structural typology. The proposed criteria are intended as data-driven strategies for structure-type classification that can be complementary to an assessment based on a-priori engineering knowledge. The continuous models used for deriving the proposed criteria are the model of a continuous bending moment-deflecting cantilever beam and the model of a continuous shear-deflecting cantilever beam, where the latter is considered as an equivalent more simplified model of the shear-type frame structure. In the first part of this section, the main dynamic features of the considered continuous cantilever beam models are briefly summarized (i.e., equation of motion under free vibration and modal parameters). Then, it is shown how such quantities were used to derive the proposed criteria for structure-type classification.

The first damage detection method presented in Sect. 2 was developed for bending moment-deflecting cantilever beam structures. Referring to building structures, a typical example is the case of a building with reinforced concrete walls connected by flexible horizontal elements, as outlined in the model shown in Fig. 2a. The walls can be modeled as cantilever beams, and it is assumed that the flexible horizontal elements can be modeled as truss elements. The whole system can be replaced by an equivalent system that is a continuous bending moment-deflecting cantilever beam. In the more general case of having a number of interconnected cantilever beams that is equal to  $b$ , the overall stiffness of the equivalent structure is

$$(EJ)_{eq} = \sum_{i=1}^b EJ_i, \tag{10}$$

where  $E$  is the modulus of elasticity (assumed as constant for each element), and  $J_i$  is the moment of inertia of the transverse cross-section of each individual cantilever beam.

The equation of motion under free vibrations of the continuous bending moment-deflecting cantilever beam [26, 27] is

$$(EJ)_{eq} \frac{\partial^4 y(x, t)}{\partial x^4} + m \frac{\partial^2 y(x, t)}{\partial t^2} = 0, \tag{11}$$

where  $m$  is the mass per unit length, which is uniform along the length  $\ell$  of the beam, and  $y(x, t)$  is the transverse displacement at time  $t$  of the section located at position  $x$ . The natural frequencies of the bending moment-deflecting cantilever beam can be evaluated as follows:

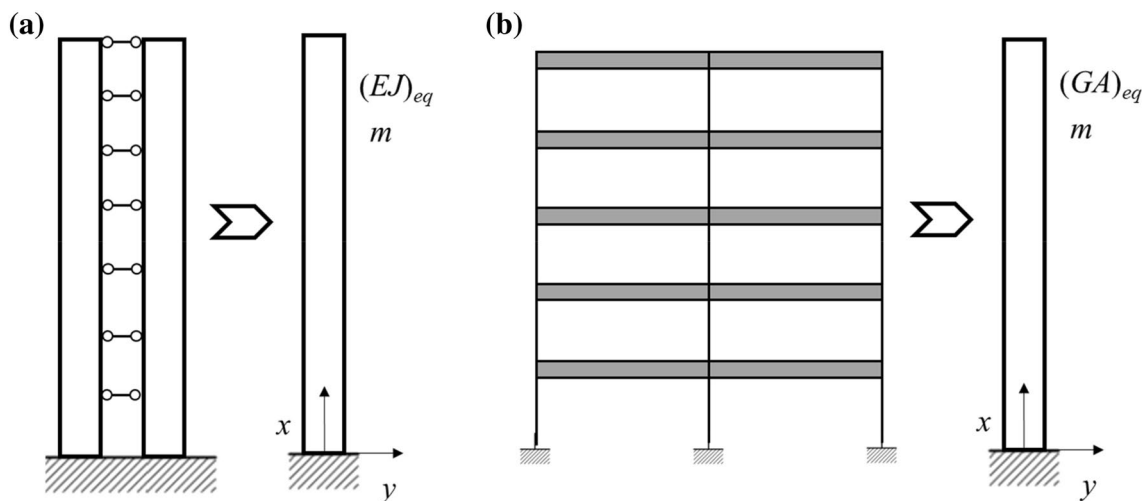


Fig. 2 Continuous cantilever beam models: **a** bending moment-deflecting cantilever beam; **b** shear-deflecting cantilever beam

$$f_1 = \frac{3.516}{2\pi} \frac{1}{\ell^2} \sqrt{\frac{(EJ)_{eq}}{m}} \text{ for } q = 1 \tag{12a}$$

$$f_q = \frac{\left(q - \frac{1}{2}\right)^2 \pi}{2\ell^2} \sqrt{\frac{(EJ)_{eq}}{m}} \text{ with } q = 2, 3, 4 \dots, \tag{12b}$$

where  $q$  is the mode number. The mode shapes of the bending moment-deflecting cantilever beam are expressed by the following function:

$$\phi_q(x) = C_1 \left[ \cos \alpha_q x - \cosh \alpha_q x - \frac{\cos \alpha_q \ell + \cosh \alpha_q \ell}{\sin \alpha_q \ell + \sinh \alpha_q \ell} (\sin \alpha_q x - \sinh \alpha_q x) \right], \tag{13}$$

where  $C_1$  is an arbitrary constant and the coefficient  $\alpha_q$  can be determined according to the following expressions:

$$\alpha_1 \ell = 1.875 \text{ for } q = 1 \tag{14a}$$

$$\alpha_q \ell = \left(q - \frac{1}{2}\right) \pi \text{ for } q = 2, 3, 4 \dots \tag{14b}$$

The second damage detection method presented in the previous section was developed for shear-type frame building structures. If the considered shear-type frame is regular in height, both in term of stiffness and mass, the dynamic behavior of such a frame can be approximated by an equivalent continuous model, which is a shear-deflecting cantilever beam with all the properties, in terms of stiffness and mass that are uniform along the length of the beam (Fig. 2b). The properties of the equivalent continuous cantilever beam can be determined from the properties of the shear-type frame through the following steps. On one side, the drift of the generic  $i$ th story of the shear-type frame model subjected to the story shear  $V_i$  can be determined as follows:

$$d_i = \frac{V_i h_i^3}{12 \sum_{w=1}^c EJ_{i,w}}, \tag{15}$$

where  $h_i$  is the interstory height,  $J_{i,w}$  is the moment of inertia of the transverse cross-section of each column, and  $c$  is the total number of the columns of the frame. On the other side, the drift of a portion of the continuous model with the same height and subjected to the same shear force is

$$\delta_i = \frac{V_i h_i}{GA}, \tag{16}$$

where  $G$  is the shear modulus and  $A = \Lambda/\kappa$ , with  $\Lambda$  that is the area of the cross-section of the beam and  $\kappa$  that is the shear factor. From Eqs. (15, 16), imposing  $\delta_i = d_i$ , the equivalent

stiffness of the continuous cantilever beam can be estimated for each story, that is

$$(GA)_{eq,i} = \frac{12 \sum_{w=1}^c EJ_w}{h_i^2}. \tag{17}$$

The equivalent stiffness for the whole shear-deflecting cantilever beam  $(GA)_{eq}$  can be assumed as the mean value over all stories of the equivalent stiffness obtained for each individual story according to Eq. (17).

The equation of motion under free vibrations of the continuous shear-deflecting cantilever beam is

$$(GA)_{eq} \frac{\partial^2 y(x,t)}{\partial x^2} - m \frac{\partial^2 y(x,t)}{\partial t^2} = 0, \tag{18}$$

where  $m$  is the mass per unit length, obtained by dividing the whole mass of the shear-type frame by the length  $\ell$  of the beam. The natural frequency of each  $q$ th mode of the shear-deflecting cantilever beam can be evaluated as follows:

$$f_q = \frac{(2q - 1)}{4\ell} \sqrt{\frac{(GA)_{eq}}{m}} \text{ with } q = 1, 2, 3, 4 \dots \tag{19}$$

The mode shapes of the shear-deflecting cantilever beam are expressed by the following function:

$$\phi_q(x) = C_1 \sin \alpha_q x, \tag{20}$$

where  $C_1$  is an arbitrary constant, and with the coefficient  $\alpha_q$  that can be determined according to the following expression:

$$\alpha_q \ell = (2q - 1) \frac{\pi}{2} \text{ for } q = 1, 2, 3, 4 \dots \tag{21}$$

In this paper, a criterion is proposed to classify the considered building structures and to select the appropriate damage detection method, and this criterion is applicable to each single experimentally identified mode shape of the structure. This proposed approach is thought to integrate the more traditional approach for structural type classification that is based on evaluating the ratios of the identified natural frequencies. This last criterion is also applied in the analyses of the present paper, as shown in the next sections.

Starting from experimentally identified natural frequencies of the structure, the frequency ratio (FR) can be evaluated as follows:

$$FR_{q1} = \frac{f_q}{f_1}, \quad (22)$$

where  $f_q$  is the natural frequency of the high-order  $q$ th mode (for  $q=2,3,4,\dots$ ) and  $f_1$  is the natural frequency of the first mode. To understand which is the structure-type and the behavior of the structure (i.e., flexural-deflecting behavior or shear-deflecting behavior), the experimentally derived frequency ratios can be compared with the reference values determined using the continuous cantilever beam models. The reference values of the frequency ratios for the bending moment-deflecting cantilever beam can be determined through the following expression:

$$FR_{EJ,q1} = \frac{f_q}{f_1} = \frac{\left(q - \frac{1}{2}\right)^2 \pi}{1.119} \quad \text{with } q = 2, 3, 4, \dots \quad (23)$$

which derives from Eqs. (12a, 12b). The reference values of the frequency ratios for the shear-deflecting cantilever beam are as follows:

$$FR_{GA,q1} = \frac{f_q}{f_1} = 2q - 1 \quad \text{with } q = 2, 3, 4 \dots \quad (24)$$

and this last expression derives from Eq. (19).

The proposed criterion for structure-type classification through the mode shapes is based on the use of proposed indices that receive in input an experimentally identified modal vector and that provide in output a scalar value. This scalar value depends upon the shape of the modal vector and can be compared with the reference values determined using the continuous cantilever beam models.

Figures 3 and 4 show the main idea that is behind the proposed criterion. In the figures, the analytical mode shapes of the first three modes of the continuous cantilever beam models are plotted: Fig. 3 shows the mode shapes of the bending moment-deflecting cantilever beam, according to Eq. (13), while Fig. 4 shows the mode shapes of the shear-deflecting cantilever beam, according to Eq. (20). It is worth noting that the analytical functions of the mode shapes do not depend on the parameters  $m$ ,  $(EJ)_{eq}$ , and  $(GA)_{eq}$ , which are uniform and constant for the whole cantilever beam. Moreover, the functions of Figs. 3 and 4 are not plotted by considering the real length of the beam (i.e., from 0 to the total length  $\ell$ ), but they are plotted as a function of a dimensionless length parameter that varies from 0 to 1.

Some mathematical operations were performed on the mode shapes, as shown in the figures. First of all, each modal vector was normalized in such a way that the component with the maximum modulus is equal to 1. Then, all the components of each mode shape were modified to have quantities that are all positive. This was done according to two different strategies, as shown in the figures. In the first case, each

component was replaced by its modulus. In the second case, each component was replaced by the squared value of the component itself.

As shown in the figures, an area is defined by the function of the modified mode shapes and the vertical axis of the plots (gray-shaded area in the figures). The extension of this area can be determined and then divided by the area of the whole rectangle that contains the modified mode shape (in Figs. 3 and 4, the area of the rectangle is equal to 1 due to the normalization adopted on the mode shape components and on the length of the beam). By performing these operations, it is possible to obtain some scalar values, indicated in the figure with the acronym NA (i.e., Normalized Area), that are constant (or at least very similar) for all the different mode shapes of each of the two considered analytical models of continuous cantilever beams. The main idea of the proposed approach for structure-type classification is thus to analyze the experimentally identified mode shapes, to estimate the scalar values of the normalized areas, and to compare the experimental results with the reference values. Such reference values, as shown in the following paragraphs, are obtained from the analytical models and can be considered as invariant quantities that can be used to discriminate between structures that have either a flexural-deflecting behavior or a shear-deflecting behavior.

When considering mode shapes that are expressed by continuous functions, the indices to be used for the estimation of the normalized areas have the following expressions. The index related to the first strategy (i.e., mode shape considered in terms of the absolute values) is as follows:

$$NA1_q = \frac{\int_0^\ell |\phi_q(x)| dx}{\ell \cdot \max(|\phi_q(x)|)}. \quad (25)$$

Equation (25) can be applied for the  $q$ -th mode shape of the structure, and this expression is further simplified when an appropriate normalization of the mode shape is considered, such that  $\max(|\phi_q(x)|) = 1$ . The index related to the second strategy (i.e., when considering the squared value of each mode shape component) is as follows:

$$NA2_q = \frac{\int_0^\ell \phi_q^2(x) dx}{\ell \cdot \max(\phi_q^2(x))}. \quad (26)$$

In the same way, Eq. (26) is also simplified in the case of an appropriate mode shape normalization, such that  $\max(\phi_q^2(x)) = 1$ .

Of course, experimentally derived mode shapes are discrete functions, not continuous functions, with the mode shape components that are defined at the instrumented locations. In the same way, mode shapes used in the numerical

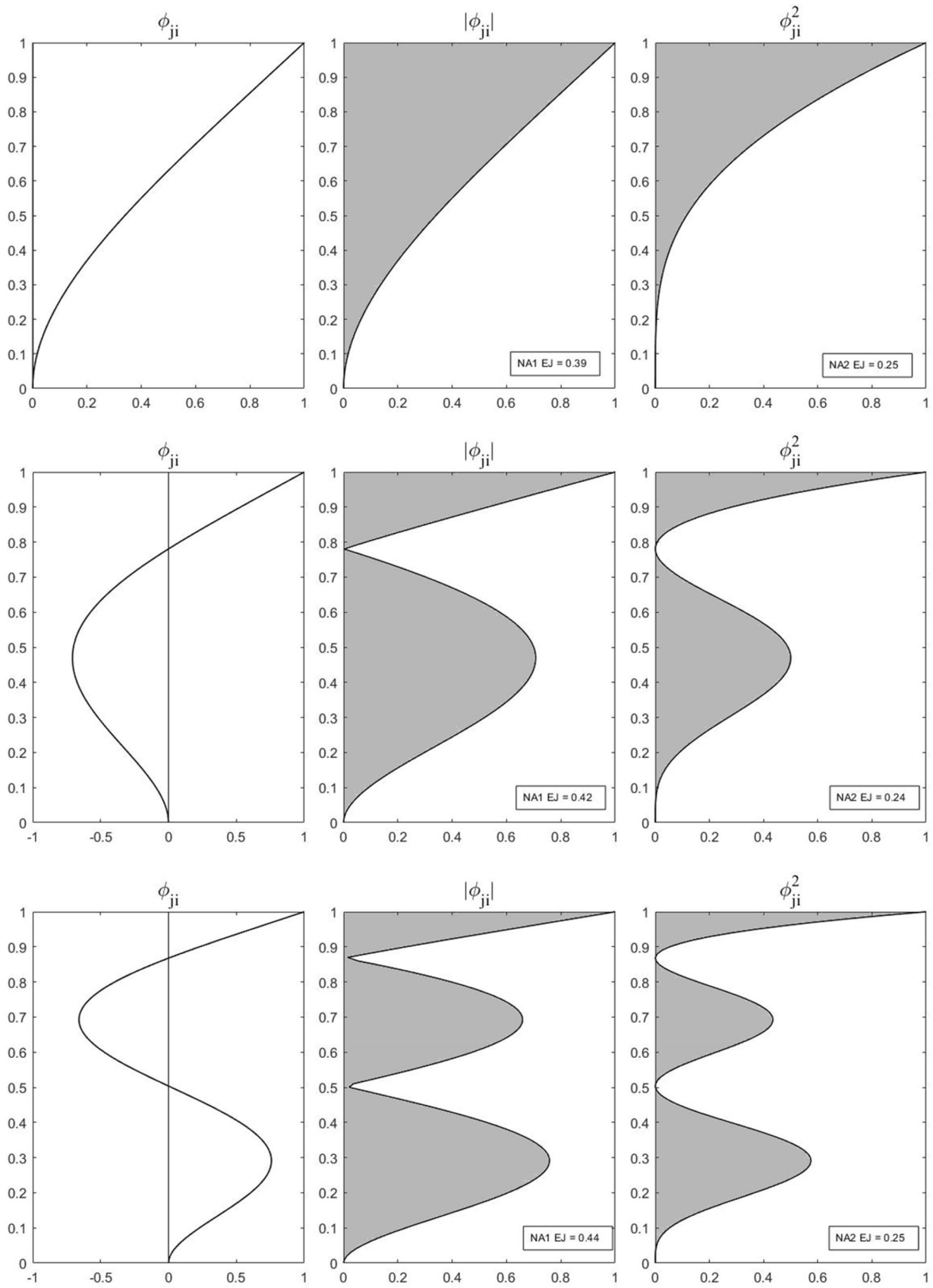
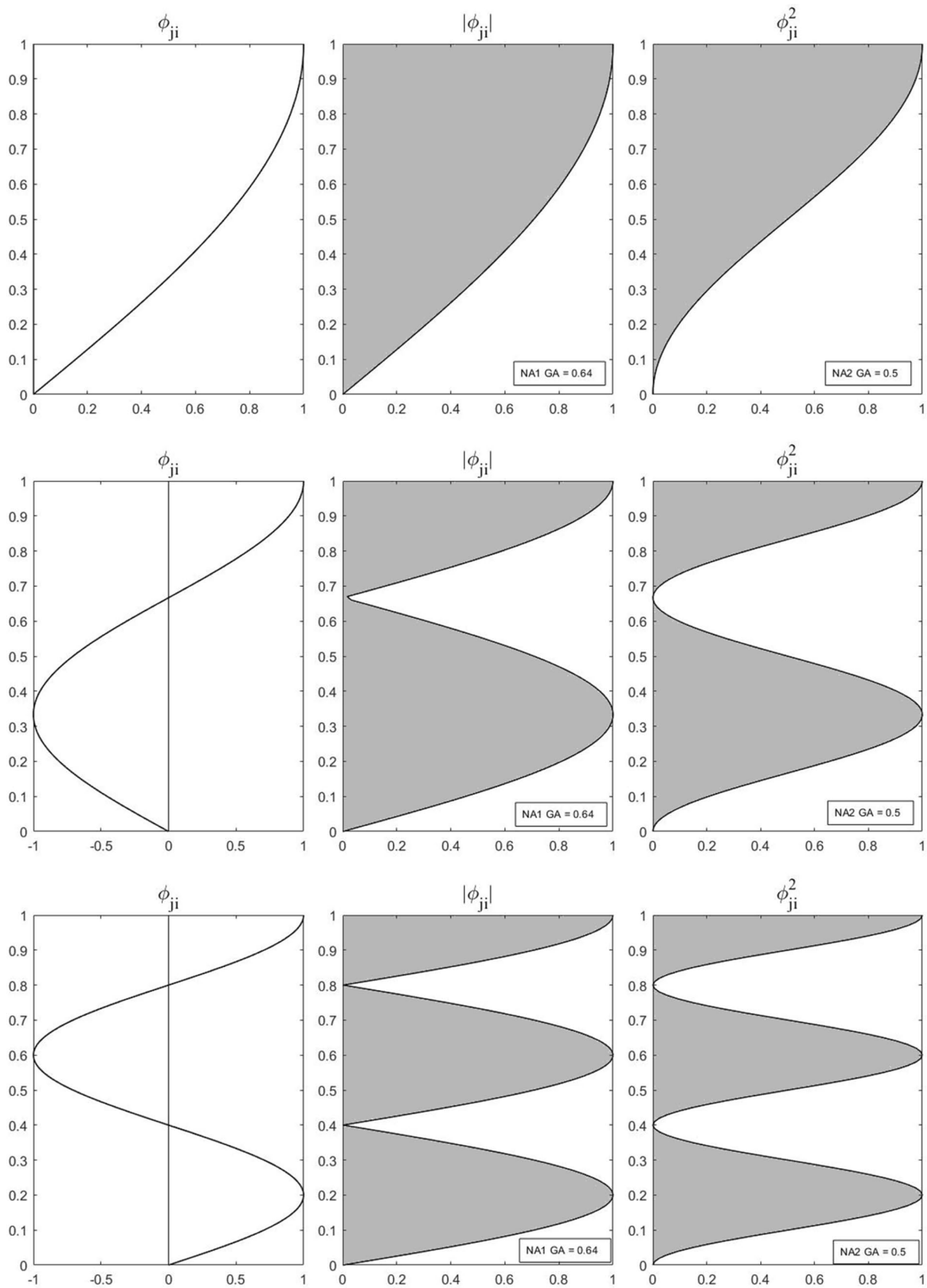


Fig. 3 Analytical model of the bending-moment-deflecting cantilever beam (EJ): mode shapes and normalized areas for the 1st, 2nd, and 3rd modes





**Fig. 4** Analytical model of the shear-deflecting cantilever beam (GA): mode shapes and normalized areas for the 1st, 2nd, and 3rd modes

analyses are also discrete quantities. In the present work, the extension of the normalized areas defined by the mode shapes was computed using the trapezoidal rule for the numerical integration. This method is more accurate than the rectangular rule, and it is a simple approach, suitable for solving the types of problems considered in this work. Moreover, the trapezoidal rule is easier to be implemented and more fast than other more complex approaches for numerical integration.

According to the trapezoidal rule for numerical integration, the extension of the area that is present beneath the function  $f(x_j)$  between extremes  $a_2$  and  $a_1$  can be evaluated using the following expression:

$$\text{area} = \frac{a_2 - a_1}{2n} \left( f(x_0) + f(x_p) + 2 \sum_{j=1}^{n-1} f(x_j) \right), \quad (27)$$

where the interval from  $a_1$  to  $a_2$  is divided in  $n$  sub-intervals of equal length. The trapezoidal rule was utilized to derive the expressions of the proposed indices NA1 and NA2, which are used in the numerical and experimental analyses of the present paper. These indices can be applied by considering mode shapes defined at  $n + 1$  points located at a constant spacing, which is the most common layout of instrumented locations adopted in practice and the case considered in all damage detection methods summarized in Sect. 2. Other more challenging cases where the points of the modal vectors are not at a constant spacing are not the key interest in the present paper and will be considered in future works.

The index related to the first strategy NA1 can be derived as follows:

$$\text{NA1}_q = \frac{\text{area}_{|\phi_q|}}{\text{area}_{\text{RECT}}}, \quad (28)$$

where the numerator is the area defined by the mode shape considered in terms of the absolute values. The extension of this area can be obtained by applying the trapezoidal rule as follows:

$$\text{area}_{|\phi_q|} = \frac{\ell}{2n} \left( |\phi_{0q}| + |\phi_{nq}| + 2 \sum_{j=1}^{n-1} |\phi_{jq}| \right), \quad (29)$$

where  $\ell$  is the length of the structure idealized as a cantilever beam, and  $\phi_{jq}$  is the generic mode shape component (with  $j = 0 \dots n$  and  $q$  that is the mode number). The denominator of Eq. (28) is the area of the rectangle that contains the modified mode shape, which is

$$\text{area}_{\text{RECT}} = \ell \cdot \max_{j=0 \dots n} (|\phi_{jq}|). \quad (30)$$

Thus, the expression for the evaluation of the index NA1<sub>q</sub> is

$$\text{NA1}_q = \frac{1}{2n} \left( |\phi_{0q}| + |\phi_{nq}| + 2 \sum_{j=1}^{n-1} |\phi_{jq}| \right) \frac{1}{\max_{j=0 \dots n} (|\phi_{jq}|)}. \quad (31)$$

The expression of Eq. (31) is further simplified when considering an appropriate normalization of the mode shapes, such that  $\max_{j=0 \dots n} (|\phi_{jq}|) = 1$ .

The same steps used for the index NA1 and the trapezoidal rule for numerical integration can be used to derive the expression for the index related to the second strategy NA2<sub>q</sub>, that is

$$\text{NA2}_q = \frac{1}{2n} \left( \phi_{0q}^2 + \phi_{nq}^2 + 2 \sum_{j=1}^{n-1} \phi_{jq}^2 \right) \frac{1}{\max_{j=0 \dots n} (\phi_{jq}^2)}, \quad (32)$$

where the squared values of each mode shape component are considered. Similarly to the case of Eq. (31), Eq. (32) is also simplified in the case of an appropriate mode shape normalization, such that  $\max_{j=0 \dots n} (\phi_{jq}^2) = 1$ .

As shown in Eqs. (31, 32), the mode shape components are the sole parameters that are needed to use the proposed indices NA1 and NA2. Moreover, each index is to be applied using a single-mode shape vector. Theoretically, such indices can thus be used even in the cases where only the first mode is identified. It is worth noting that, on the contrary, the criterion based on the evaluation of the ratios of the natural frequencies (mentioned in previous paragraphs) also require the knowledge of the high-order modes.

To identify the reference values that the proposed indices NA1 and NA2 assume for a bending moment-deflecting cantilever beam and a shear-deflecting cantilever beam, the calculations of Eqs. (25, 26) have to be applied for the analytical expressions of the mode shapes of Eqs. (13, 20). In the present paper, this problem was solved numerically by applying the trapezoidal rule for numerical integration. The functions of the mode shapes of Eqs. (13, 20) were evaluated by considering beams with a unitary length that is discretized in 100 sub-elements. This corresponds to 100 sub-intervals (i.e., 101 points) to apply the numerical integration. Then, the values of the normalized areas were evaluated using the trapezoidal rule and using Eqs. (31, 32). It is worth noting that the considered discretization was deemed sufficient to obtain accurate results, since increasing the number of sub-intervals did not bring to modifications and improvements in the obtained results.

The results are provided in Table 1 for the first ten mode shapes of both the bending moment-deflecting cantilever beam and the shear-deflecting cantilever beam. As shown in the table, for the shear-deflecting cantilever beam, the values of the normalized areas are constant for each mode both for the first index NA1 and the second index NA2. This

**Table 1** Values of normalized areas for the analytical models: length of the cantilever beam discretized in 100 sub-intervals

	Mode	1	2	3	4	5	6	7	8	9	10
NA1	GA	0.637	0.637	0.636	0.637	0.637	0.637	0.637	0.636	0.637	0.637
	EJ	0.392	0.423	0.437	0.441	0.443	0.444	0.445	0.446	0.446	0.447
NA2	GA	0.500	0.500	0.500	0.500	0.500	0.500	0.500	0.500	0.500	0.500
	EJ	0.250	0.244	0.250	0.250	0.250	0.250	0.250	0.250	0.250	0.250

is a result that can also be verified by solving the definite integrals of Eqs. (25, 26) for the case of the sine function mode shape of Eq. (20). For the bending moment-deflecting cantilever beam, the values of normalized areas are not identical for all modes (differently from the case of the shear-deflecting cantilever beam), but such values for the EJ beam are in any case very similar when considering the different modes, especially for the second index NA2. In fact, for the EJ beam NA1 is 0.39 for the first mode and then tends to 0.45 for high-order modes, while NA2 is approximately equal to 0.25 for all modes.

The performed calculations were thus useful to identify the reference values that the proposed indices NA1 and NA2 assume for the two considered cantilever beams. For the bending moment-deflecting cantilever beam, the identified reference values are

$$NA1_{EJ} = 0.39 \div 0.45; \quad NA2_{EJ} = 0.25. \quad (33)$$

For the shear-deflecting cantilever beam, the reference values are

$$NA1_{GA} = 0.64; \quad NA2_{GA} = 0.5. \quad (34)$$

According to the proposed approach, the indices of Eqs. (31, 32) can thus be evaluated by considering experimentally derived mode shapes. Then, the estimated values of normalized areas can be compared with the reference values indicated in Eqs. (33, 34) to perform the structure-type classification and to understand which is the behavior of the structure (i.e., flexural-deflecting behavior or shear-deflecting behavior).

Referring to the reference values of the indices shown in Eq. (33) for the EJ beam, it is important to note the effect that is generated when considering the squared values of the mode shape components (NA2) instead of the modulus of the mode shape components (NA1): the range that describes the reference solutions for  $NA1_{EJ}$  is transformed into a fixed reference value for  $NA2_{EJ}$ . In general, it can also be inferred that the use of the squared values of the mode shape components (NA2) tends to amplify the differences between the values of the indices associated with the EJ and GA beams. In fact, as shown in Eqs. (33, 34), the value of  $NA2_{GA}$  is two times the value of  $NA2_{EJ}$ , while, on average, the value of  $NA1_{GA}$  is one and a half times higher than the solution obtained for  $NA1_{EJ}$ . These observations suggest that, from

the theoretical point of view, the index NA2 might be more effective than the index NA1.

It is important to study how the proposed indicators behave when the mode shapes are defined at a limited number of points (much less than the number of points considered in the previous analysis performed to obtain the reference values), as this is the case that more frequently occurs in real experimental tests. To this purpose, a parametric analysis was performed by considering analytical functions of the mode shapes (Eqs. 13, 20) that are sampled in different scenarios with an increasing number of sub-intervals. The number of sub-intervals is the parameter  $n$  (which corresponds to mode shape components defined at a number of points equal to  $n + 1$ ), and the analyses were repeated for  $n$  that assumes each value from 1 to 15. Both for the bending moment-deflecting cantilever beam and the shear-deflecting cantilever beam, the first four modes were considered in this analysis. The proposed indices NA1 and NA2 were evaluated according to Eqs. (31, 32), using the trapezoidal rule for numerical integration, and the results of the parametric analysis are shown in Fig. 5.

In Fig. 5, it can be observed that in some cases where the number of sub-intervals is very low, the values of the indices NA1 and NA2 are not equal to the expected reference values. With a very low number of sub-intervals, there are also cases where the index related to the EJ beam is equal (or very similar) to the index related to the GA beam (as evident for example both for NA1 and NA2 when considering the third mode evaluated with a number of sub-intervals equal to 3, i.e., a number of mode shape components equal to 4). This is an inevitable effect that occurs when the number of sub-intervals and points is not sufficient to adequately describe the shape of the modal vector. On the contrary, when the shape of the modal vector is adequately described using a higher number of sub-intervals (and points), the values of the indices NA1 and NA2 tend to converge to the reference values shown in Table 1. The higher the order of the mode shape, the higher the number of the inversions in the signs of the mode shape components, which is associated with shapes of the modal vectors that are more complex. This affects the results of Fig. 5 where it is indeed evident that the indices for the low-order modes converge more rapidly to the reference values than those related to the high-order modes. It is important to emphasize that the trend associated with the index NA1 (that uses the modulus of each mode shape

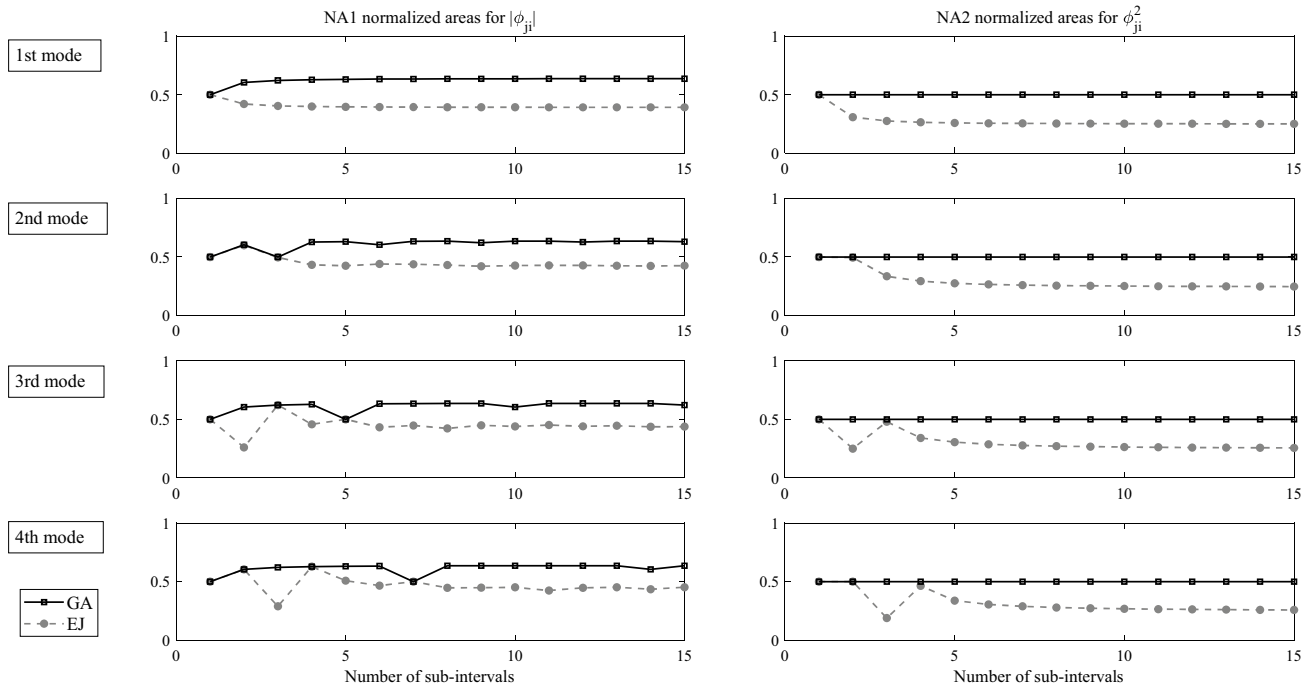


**Fig. 5** Parametric analysis for the two cantilever beam models: values of normalized areas expressed as a function of the number of sub-intervals used to sample the analytical functions of the mode shapes

component) is different to the trend related to the index NA2 (that uses the squared value of each mode shape component). Specifically, the performed analyses of Fig. 5 show the following general rule. Referring to the index NA1, if one considers a generic  $q$ th mode, at least  $2q$  sub-intervals are needed to start to have a clear separation between the values of the index associated with the EJ and the GA beams and to have a convergence toward the reference values. On the contrary, for the index NA2, the same result for a generic  $q$ th mode is reached when considering a number of sub-intervals that is at least  $q + 1$ . This last number ( $q + 1$  for NA2) is lower than the value obtained for NA1 (i.e.,  $2q$ ), except for the first mode. This suggests that the index NA2 might be more effective than the index NA1, especially when considering the high-order modes.

Other two observations can be made about the results of Fig. 5. First, it is interesting to note that for the first mode, the values of both NA1 and NA2 tend to be similar to the reference values for any number of considered sub-intervals (with the obvious exception of the case with one sub-interval—i.e., mode shape described by only two points—where there is clearly not enough information to discriminate between the EJ and the GA beams and where the normalized area is equal to 0.5 both for NA1 and NA2). Second, it is also interesting to note the different behavior that the two indices (NA1 and NA2) have when considering the GA beam. The index NA2 is always equal to 0.5 for any of the considered number of sub-intervals (and for

any of the considered modes). On the contrary, the value of the index NA1 is not constant: it is equal to 0.5 with only one sub-interval and then converges to the reference value 0.64 for a higher number of sub-intervals. The parametric study of Fig. 5 confirms, from the theoretical point of view, the applicability of the proposed criterion for mode shape-based structure-type classification and, as outlined in this paragraph, gives indications about the minimum number of points that are needed to properly define the shape of the modal vectors and to properly use the proposed indices NA1 and NA2.

Overall, the observations derived from the analyses shown in this section suggest that, from the theoretical point of view, the index NA2 might be more effective than the index NA1. The indices were, in any case, both developed on the common idea of evaluating the normalized areas generated by the modal vectors, and the differences between the two indices are only due to the different mathematical operations applied on the mode shape components (i.e., evaluating the modulus for NA1 and evaluating the squared value for NA2). For comparison purposes, the indices NA1 and NA2 were both applied to the experimental case studies shown in the next section.

The criteria for building structure-type classification proposed in this paper and, specifically, in this section address the types of structures that can be analyzed using the existing method for damage detection shown in Sect. 2. It is worth mentioning that the present paper does not address more

complex structures such as the building structures where there is a combined use of RC walls and RC frames. These structures can be usually modeled by coupling a bending moment-deflecting cantilever beam and a shear-deflecting cantilever beam, and their dynamic behavior is in general more complex than the structures considered in this paper. The study of such more complex structures, addressing for example both the structure-type classification and the damage detection, is part of a larger problem that will be the object of future developments of the research. In general, for structures that do not present a clear bending moment or shear-deflecting behavior, it is expected that analyzing the changes in the modal flexibility-based deflections could give useful information about the presence of potential damage, and an attempt could be made in future research to develop specific deflection-based indicators for damage localization. To increase the reliability and the robustness of the damage detection process when applied to such more complex structures, it could also be useful to integrate the results of the deflection-based method with the outcomes of other modal flexibility-based methods (e.g., change in flexibility method [5] or damage locating vector method [28]).

The proposed criteria to identify the structural type could be used in the other contexts than for selecting the most appropriate flexibility-based algorithms and DSFs for damage detection. The proposed criteria could be used in the context of dynamic tests (e.g., ambient vibration tests) performed to verify the design of a new construction or to gain knowledge about an existing structure (for safety assessment or for designing retrofit interventions). In these situations, the proposed indices could be considered as simple data-driven tools that can be used to support and confirm the evaluations made by the structural designer about the behavior of the structure and the modeling assumptions. The proposed indices could be particularly helpful in the case of a complex structural system where it is of interest to understand to which extent the structural behavior is close to that of an ideal model (e.g., an ideal model with bending-moment-deflecting behavior or an ideal model with shear-deflecting behavior).

#### 4 Application to full-scale reinforced concrete buildings

The structure-type classification criteria and the damage localization approaches described in the previous sections were applied on the data of experimental tests that were performed on full-scale reinforced concrete structures that experienced earthquake-induced damage. Two structures are considered in this section of the present paper: the first one is a seven-story RC wall building, while the second structure is a five-story RC frame building. Both structures were

tested at the Englekirk Structural Research Center using the University of California–San Diego Network for Earthquake Engineering Simulation (UCSD-NEES) large outdoor unidirectional shake table.

##### 4.1 Seven-story RC wall building

The first case study is a slice of a full-scale seven-story RC building with cantilever structural walls acting as a lateral force resisting system (Figs. 6, 7). It was tested between September 2005 and May 2006 using a unidirectional shake table to simulate earthquake-induced damage. The building was 19.20 m high and consisted of two perpendicular walls in elevation (i.e., web and flange walls) with a horizontal RC slab at each level. An auxiliary post-tensioned column provided torsional stability and four gravity columns supported the slabs. The structure was positioned on the shake table with the main longitudinal wall aligned with the direction of the base excitation (i.e., the east–west direction). A dense array of sensors was deployed on the specimen, including accelerometers. During the experimental campaign, some historical earthquake records were applied at the base of the structure to induce progressive damage. After each strong motion test, low-amplitude white noise base excitation (3%g root mean square—RMS) tests and ambient vibration tests were performed for damage characterization purposes. More detailed information about the structure and the performed



Fig. 6 Test structure: a slice of a seven-story RC wall building [32]

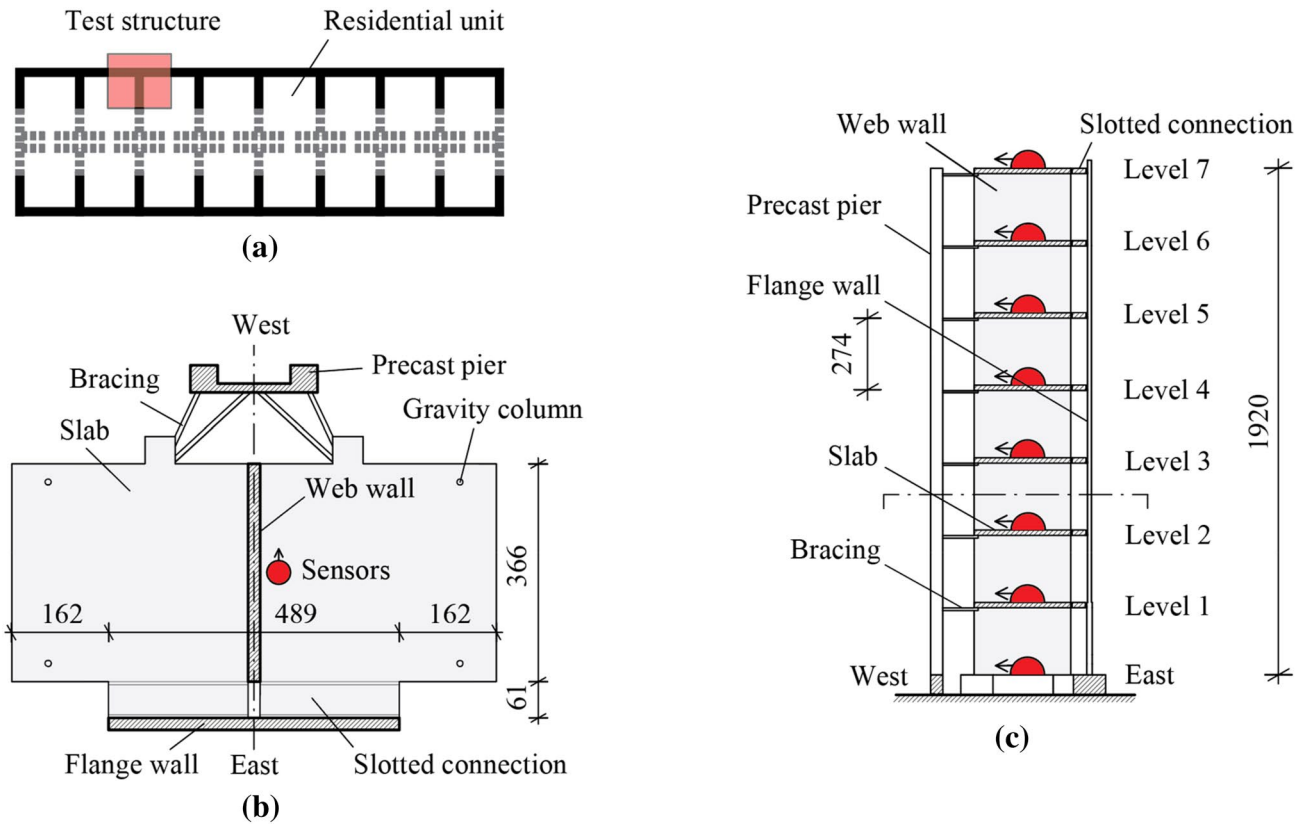


**Fig. 7** Schematic drawing of the geometry of the structure with indications of the instrumented locations (geometry retrieved from [29, 32], dimensions in cm): **a** floor plan view of the building; **b** floor plan view of the test structure; **c** elevation of the test structure

vibration tests can be found in [29–31]. Moreover, the data used in this section are available at [32].

In this study, only vibration datasets (of 8 min each) collected during the mentioned low-amplitude white noise tests were considered. Specifically, the following configurations were studied: S0, which is the baseline configuration; S1, which is the damaged state resulting from the application of the longitudinal component of the San Fernando earthquake measured in 1971 at the Van Nuys station; S2, which is the damaged state obtained by the transversal component of the mentioned San Fernando earthquake; S3.1, a damaged state generated by subsequently applying the longitudinal component of the Northridge earthquake measured in 1994 at the Oxnard Boulevard station in Woodland Hill. Moreover, only accelerometers positioned near the main longitudinal wall and oriented in the direction of the base excitation (Fig. 7) were considered in the analyses. All the measurements used for the analyses have a sampling frequency ( $f_s$ ) of 240 Hz.

The damage observed visually (i.e., from pictures and video recordings) and from strain sensors during the experimental tests is herein briefly reported to have an idea of the expected results for the damage identification process. As described in [30], the damage is concentrated at the lower two stories of the longitudinal web wall. This description

matches the outcome of the vibration-based identification procedure applied in [30] using acceleration measurements. From a finite-element (FE) model updating and analyzing the strain data, the authors of the mentioned reference confirmed that the extent of damage increases as the structure is exposed to stronger earthquake excitations.

In this study, first, the acceleration measured at the base of the structure was subtracted from the acceleration collected at each instrumented DOF to obtain a relative measurement. Then, the Eigensystem Realization Algorithm (ERA) [33] combined with the Natural Excitation technique (NExT) [34] was employed to identify the modal parameters of the structure. The dataset collected in the baseline condition was divided into eight portions of 1 min each, all employed individually to estimate the modal parameters. This process was carried out to estimate the degree of variability that affects the quantities identified in the baseline state, which is a fundamental step required for applying the subsequent statistical approaches for damage localization. It is worth noting that 8 is not the optimal number of samples for the assumed normal distribution model. However, given the duration of the dataset relevant to the 3%g RMS white noise base excitation tests, this choice resulted from a trade-off between the number of portions and their time length. In

general, it was possible to identify the first three longitudinal modes in the direction of the applied white noise base excitation for all the structural states. The natural frequencies identified for the different states of the structure are provided in Table 2, where the parameters of the baseline state S0 are provided in terms of averaged values.

The criteria for structural type classification presented in Sect. 3 were applied using the modal parameters for the baseline state S0. Figure 8 presents the analysis performed using the proposed approach based on the normalized areas for the first mode shape of the structure: the figure shows the identified mode shape (Fig. 8a) and how such mode shape is modified to evaluate the normalized areas—i.e., in one case, the modulus of the components is considered (Fig. 8b); in the other case, the squared values of the modal components are plotted (Fig. 8c). Of course, Fig. 8a and b are identical, since the first modal vector has no sign inversions in its components. Figure 8 also shows the values of the indices NA1

and NA2 calculated from the identified modal vector. All the quantities presented in Fig. 8 are compared with the reference values obtained from the analytical models of the two cantilever beam models (i.e., the EJ beam and the GA beam). From the comparison, it is evident that, for the considered experimental case study, the obtained values of the indices (both NA1 and NA2) are close to the reference solutions of the bending-moment-deflecting cantilever beam.

The same analysis was performed also for the high-order mode shapes, and the values of NA1 and NA2 obtained for all the identified modes are shown in Table 3. It can be observed that the values of NA1 and NA2 obtained for the 2nd and 3rd modes are higher than those related to the 1st mode. Moreover, the indices for the 2nd and 3rd mode shapes tend to be close to the reference solutions of the GA beam, and this appears to be not in agreement with the results obtained for the 1st mode shape. The outcomes obtained using the NA indices were examined in more detail by a graphical comparison between the identified and analytical mode shapes (presented in Fig. 9 for all the modes). The figure confirms that the 1st identified mode shape is close to the solution of the EJ model, and a clear separation is evident with respect to the mode shape of the GA model.

**Table 2** Identified natural frequencies of the 7-story building in the different states

State	Natural frequency $f_i$ [Hz] (% variation w.r.t. baseline state S0)		
	1st mode	2nd mode	3rd mode
S0 <sup>a</sup>	1.69	11.53	24.81
S1	1.53 (− 9.8)	11.32 (− 1.9)	24.67 (− 0.6)
S2	1.23 (− 27.3)	10.56 (− 8.4)	23.41 (− 5.6)
S3.1	1.11 (− 34.4)	7.88 (− 31.6)	19.72 (− 20.5)

<sup>a</sup>Mean values of natural frequencies

**Table 3** Values of normalized areas for the 7-story building

Mode	Experimental case—7 story building			Reference values	
	1	2	3	EJ	GA
NA1	0.43	0.58	0.63	0.39–0.45	0.64
NA2	0.29	0.45	0.52	0.25	0.50

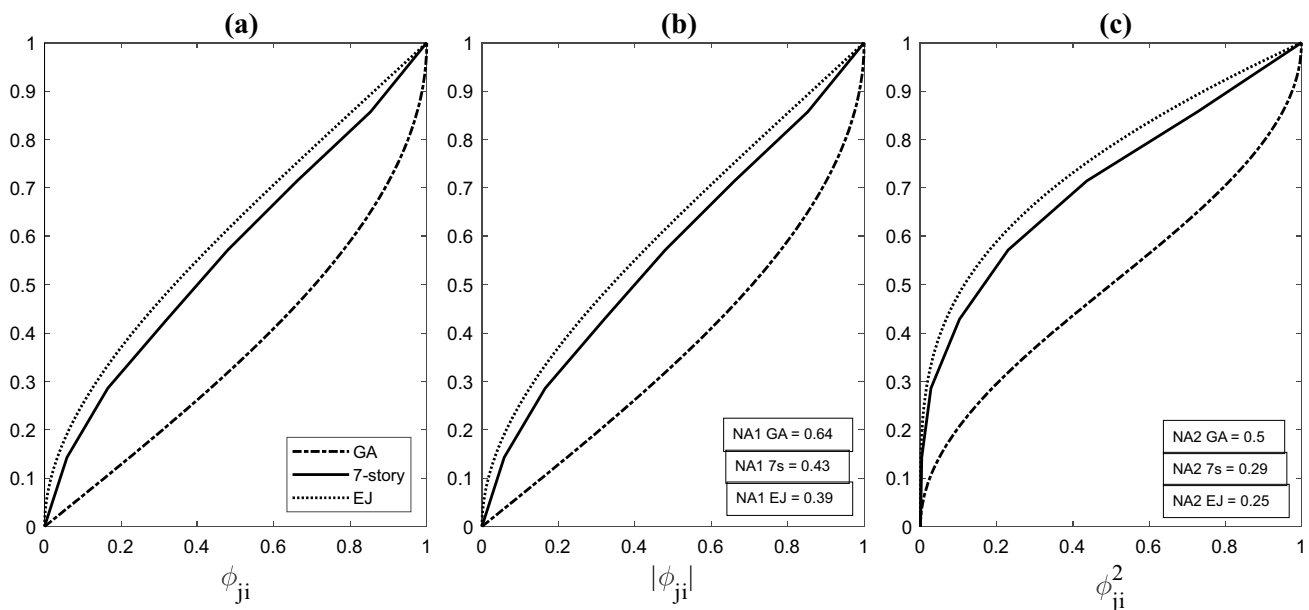


**Fig. 8** Mode shape (a) and normalized areas (b, c) for the first mode of the 7-story building (results compared with the analytical models)

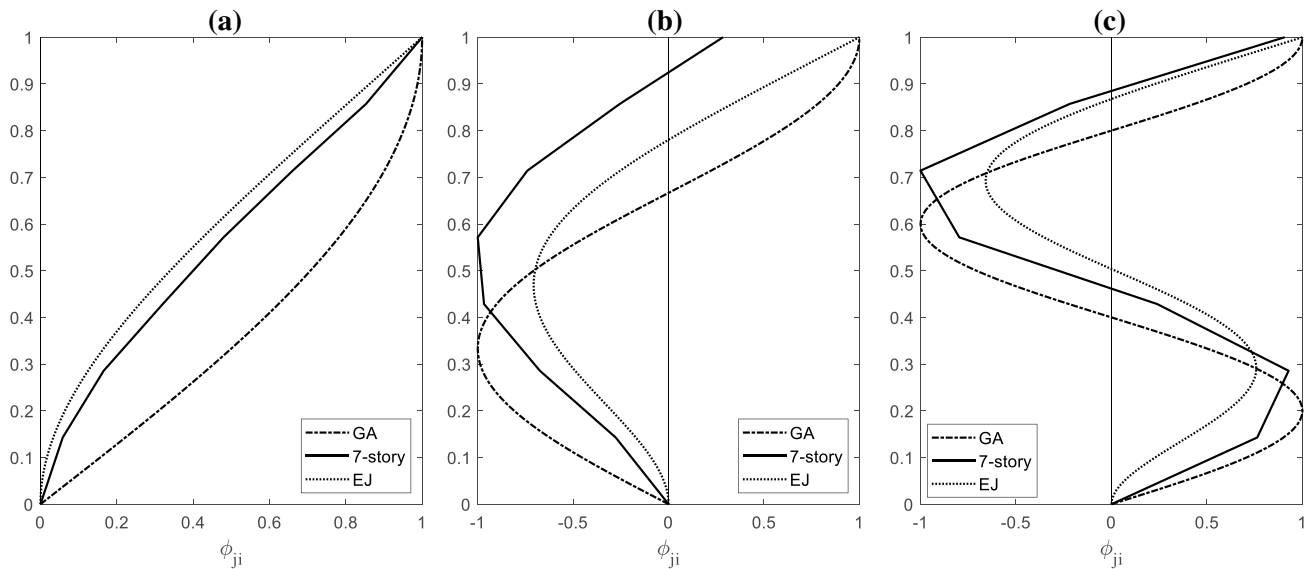


**Fig. 9** Mode shapes for the 7-story building and comparison with the analytical models: **a** 1st mode; **b** 2nd mode; **c** 3rd mode

**Table 4** Ratios of the natural frequencies for the 7-story building and comparison with the analytical models

State $S_0$	Natural frequency ratios	
	$f_2/f_1$	$f_3/f_1$
Experimental case—7 story building	6.82	14.68
Analytical model—EJ cantilever beam	6.32	17.54
Analytical model—GA cantilever beam	3	5

On the contrary, for the 2nd and 3rd modes of the considered experimental case study it seems to be difficult to associate each identified mode shape to one model or the other (especially for the 3rd mode), and this is consequently reflected on the values of NA1 and NA2 shown in Table 3. Considering the obtained results, considering that for any cantilever beam, the contribution of the first mode to the response is usually greater than the high-order modes, and considering that in the identification process, the first mode is usually identified more accurately, it can be deduced that the analyzed structure has a behavior that is more similar to the EJ beam model. This is also confirmed by the analysis of the ratios between the natural frequencies of the structure, which are provided in Table 4, together with the reference solutions of the analytical models obtained with Eqs. (23, 24). As shown in the table, the frequency ratios of the seven-story building match the ratios related to the EJ cantilever beam.

After performing structural type classification, the flexibility deflection-based method was applied for damage detection (as outlined in Sect. 2), by considering the deflection curvature as a damage-sensitive feature. The identified

modal parameters were employed to assemble the modal flexibility matrices of the structure in the different states using Eq. (1). The mass matrix was estimated a-priori using available information and used to calculate the mass normalization factors of identified modes. In the evaluation of the mass matrix of the beam-like cantilever structure, the rotational inertia was neglected, and the mass was considered uniformly distributed along the height of the structure. This resulted in estimating a diagonal mass matrix with non-zero components proportional to the structural masses relevant to the measured DOFs. Using a proportional mass matrix led to estimating proportional flexibility matrices, used to evaluate the modal flexibility-based deflections. This was done according to Eq. (2), considering a uniform load with unitary values at all the measured DOFs as the inspection load.

The modal flexibility-based deflections of the structure identified in different states are reported in Fig. 10. Specifically, the displacements, rotations, and curvatures of the deflections are reported in Fig. 10a–c, respectively. In general, the deflections derived experimentally, as well as their derivatives, are in agreement with the corresponding quantities expected from a bending moment-deflecting cantilever beam model loaded by uniform loads, even if some more irregular trends are inevitably present in the experimental results. Curvature estimates shown in Fig. 10c tend to increase in the lower DOFs, as expected. However, an inversion in the curvature at DOF number 6 can be observed, while the curvature goes to zero at DOF number 3. These effects and more irregular trends observed in the experimental results could also be due to inevitable uncertainties related to the process of estimating the curvature of experimental deflections using the approximated finite difference



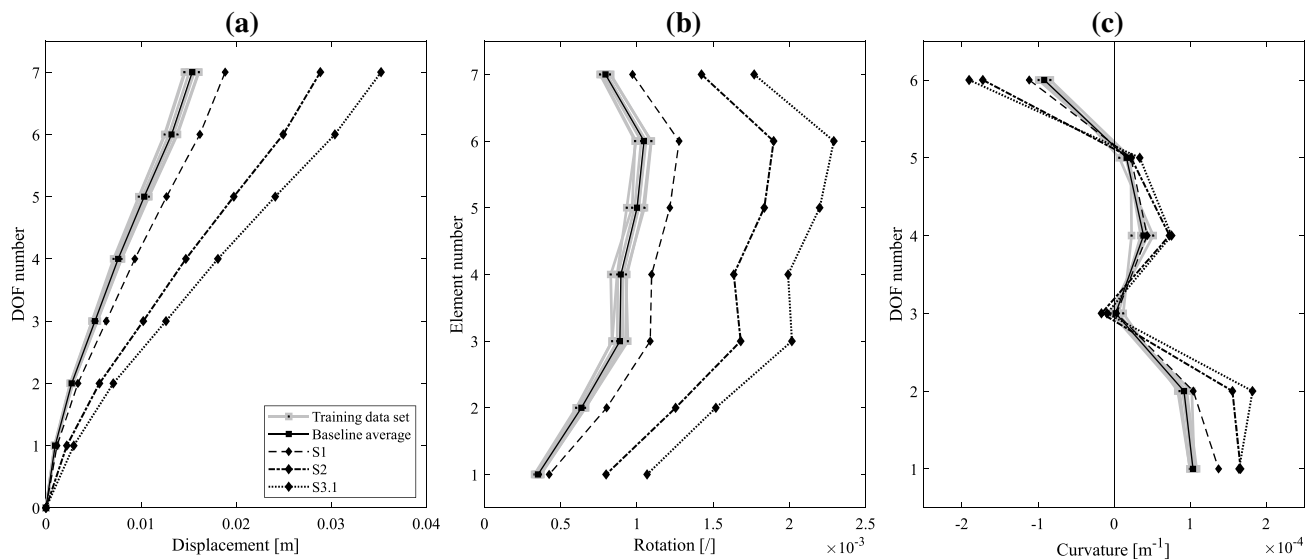


**Fig. 10** Modal flexibility-based deflections of the 7-story building: **a** displacements; **b** rotations; **c** curvatures

method, according to Eq. (6). Moreover, Fig. 10a shows that the displacements increase progressively when considering, in the order, the baseline state and the states S1, S2, and S3.1. This is a clear indication that structural modifications have occurred between the different states. Indeed, since these deflections were calculated using the same inspection load, a gradual stiffness decrement is evident. The values of the natural frequencies for the different states also confirm that structural modifications have occurred. From Table 2, it can be observed that the frequencies related to the states S1, S2, and S3.1 (i.e., the damaged states) are lower than the frequencies of the baseline structure, as expected. Moreover, the frequencies progressively decrease when considering structural states characterized by more severe damage.

The results of damage localization are reported in Fig. 11, where Fig. 11a shows the damage-induced curvature (i.e., the difference between the curvature in the damaged state and the curvature in the baseline state), while Fig. 11b shows the results obtained using the  $z$ -index based on curvature (Eq. 7). The quantities shown in Fig. 11a and b have a similar trend, and indeed, a relationship exists between the two quantities: the damage-induced curvature is the numerator of Eq. (7), which is the expression of the  $z$ -index where the statistical variability of the baseline DSFs is appropriately considered. Figure 11 provides results in terms of damage localization that are consistent with the actual damage observed during the experimental campaign, which, as mentioned in [30], is concentrated at the bottom two stories of the structure. In particular, through the adopted  $z$ -index, it is possible to detect the DOFs of the structure that have been affected by the damage. It can be observed from Fig. 11b that the values of the  $z$ -index at the upper DOFs are lower

than the corresponding values at the bottom of the structure. The values of  $z$ -index at the DOF number 3, 4, 5, and 6 are in general below the threshold, except for some cases where the  $z$ -index is slightly higher than the threshold (such cases shown in Fig. 11b can be considered as false positives). It is worth noting that Fig. 11 shows some negative values of the damage-induced curvature and the  $z$ -index at DOF number 6, and such values are due to the irregular trend of the curvature at the same DOF already discussed for Fig. 10c. The considered  $z$ -index is thought for performing statistical tests for damage detection and localization, and it was not explicitly derived for damage quantification purposes. However, the results presented in Fig. 11 clearly show that the values of the  $z$ -index (and also the values of the damage-induced curvature) tend to increase for states that have undergone a higher number of earthquake excitations (i.e., considering in the order the states S1, S2, and S3.1), and this is consistent with the observations provided in [30].

## 4.2 Five-story RC frame building

The second case study is a five-story RC building comprising structural and nonstructural elements, simulating a complete real building, tested on the UCSD-NEES shaking table between May 2011 and May 2012 (Fig. 12). The plan dimensions of the entire structure were  $6.60 \times 11.00$  m and the floor-to-floor distance was 4.27 m, with a total height of the building of 21.34 m, as shown in the scheme of Fig. 13. The shake motion was impressed in the longitudinal (east–west) direction, in which the building had two RC frames as a lateral-load resisting system, made of rectangular beams with a cross-section of  $0.30 \times 0.71$  m and rectangular columns of

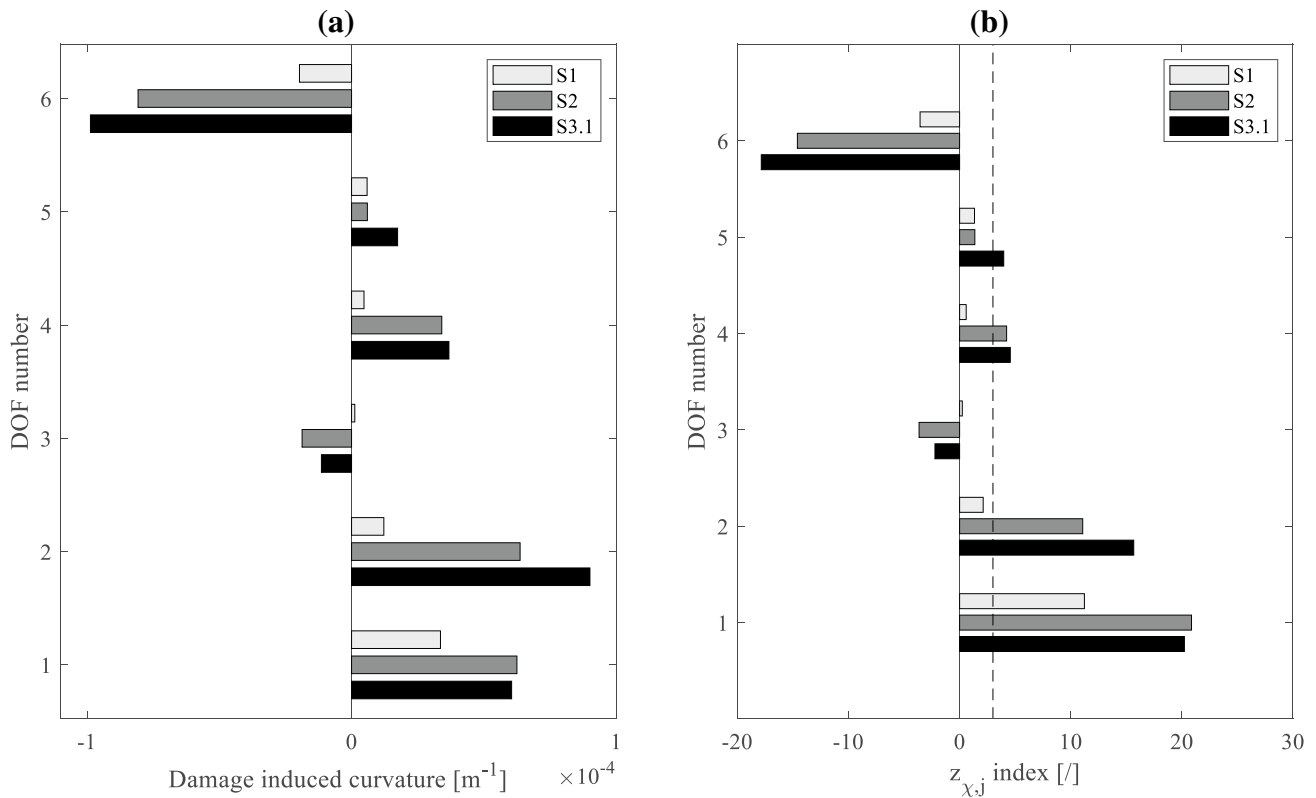


**Fig. 11** Damage detection and localization for the 7-story building: **a** damage-induced curvature; **b** z-index based on curvature (where the dashed line represents the threshold value)



**Fig. 12** Five-story RC frame building [40]

0.46 × 0.66 m. The floor system consisted of 0.20 m-thick concrete slabs.

A dense sensor equipment was originally deployed on the structure. In this study, only the accelerometers positioned in the northern-eastern and southern-eastern quadrants of the plant, at the floor level, were used, selecting the recording channels in the direction of the seismic motion. Specifically, the acceleration time histories used in this study were obtained for each level of the building by averaging the data collected in the two quadrants. More details on structural and nonstructural apparatus, as well as the sensing setup, can be found in [35–39]. Moreover, the data used in this section are available at [40].

During the experimental campaign, the structure was first tested with base isolator devices, and then subjected to six seismic motions with increasing intensity with the basement of the building fixed to the shake table. After each seismic motion, white noise motions with different amplitudes and double-pulse inputs were impressed at the base of the specimen. In this study, only the datasets collected during the white noise tests were employed to study the structural behavior in the following configurations: C0, which is the baseline configuration; C1, which is the damaged state resulting from the application of the Pisco earthquake (Peru)

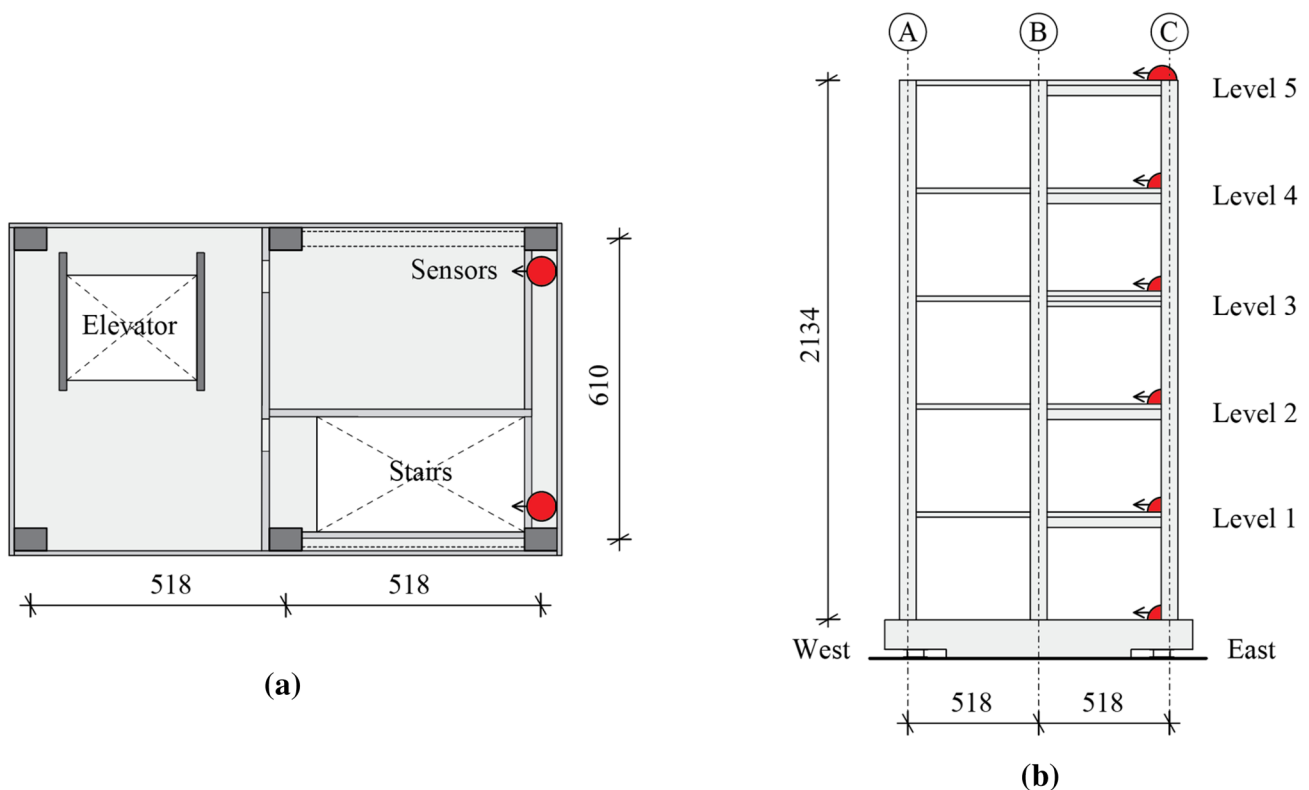


**Fig. 13** Schematic drawing of the geometry of the 5-story building with indications of the instrumented locations (geometry retrieved from [40], dimensions in cm): **a** floor plan view; **b** elevation

measured in 2007 at the Ica station; C2, which is the damaged state resulting from the following application of the Denali earthquake measured in 2002 at the TAPS Pump Station #9, rescaled at 67%. Specifically, two datasets were used to identify the modal parameters in the configuration C0, collected during 3%g and 3.5%g RMS white noise excitation, respectively, both with a duration of 6 min. On the other hand, the modal parameters of configuration C1 were identified using a dataset collected during 3%g RMS white noise excitation, and the modal parameters of configuration C2 were identified using a dataset collected during 3.5%g RMS white noise excitation. These last two datasets have a duration of 4 min. The damage indices presented in this paper were obtained by comparing the modal parameters identified in configurations C1 and C2 with those identified in configuration C0 using the datasets with the same RMS amplitude as the damaged configurations. The original sampling frequency of the considered datasets was of 200 Hz, downsampled at 100 Hz in this study.

As described in the reports of the experimental campaign [36], limited structural cracking was observed following the application of the Pisco earthquake, predominantly concentrated at the bases of the first floor columns of the north frame, with minimal cracking in the other columns. On level two, further cracking developed in the slab, and only some

columns and some beams developed cracks. The building was designed to reach its performance targets during the scaled Denali earthquake, after which the structural elements presented extensive cracks throughout their heights, and especially at the lower floors, with spalling of the concrete cover. On level two, existing cracking propagated in some parts of the slab, showing signs of an imminent punching shear failure. Overall, as described in [39], the damaged state that resulted from the application of the Pisco earthquake (i.e., configuration C1 in this paper) is characterized by minor flexural cracking on the columns at stories 1–2 and on the North beam of floors 2–3. The damaged state due to the subsequent application of the scaled Denali earthquake (herein configuration C2) was more severe, and it is globally described in [39] as characterized by moderate flexural cracking on the same structural elements.

Similarly to the previous case study, the absolute accelerations recorded at each floor level were transformed into relative accelerations, evaluated with respect to the base of the structure. Moreover, the modal parameters were identified using the NExT-ERA algorithm [33, 34], by segmenting the training data set into different portions to evaluate the statistical variability of the baseline state. The first three longitudinal modes in the direction of the applied white noise motion were identified, and the results are reported in

Table 5 (where mean values are shown for the undamaged configuration C0).

The modal parameters of state C0 were used to apply the criteria for structure-type classification. Figure 14 shows the analyses performed for the first mode shape, and its contents are presented in the same way of Fig. 8, already discussed for the first case study. Among the two reference solutions (i.e., EJ and GA beams), the trends of the identified mode shape and the curves derived from the mode shape itself are more similar to the reference solution for the GA beam. In the same way, the values of NA1 and NA2 for the identified mode shape are closer to the reference NA values of the GA beam than they are with respect to the NA values for the EJ beam. The values of the indices NA1 and NA2 are provided in Table 6 for all identified modes. For the 2nd and 3rd modes, the values of NA1 and NA2 are closer to the reference solutions for the GA beam than they are with respect to the solutions of the EJ beam: for the 2nd mode, a good match is found between the identified NA values and those

**Table 6** Values of normalized areas for the 5-story building

Mode	Experimental case—5story building			Reference values	
	1	2	3	EJ	GA
NA1	0.55	0.60	0.76	0.39–0.45	0.64
NA2	0.40	0.47	0.66	0.25	0.50

of the GA beam, while for the 3rd mode, the values of NA1 and NA2 are slightly higher than the reference solutions. The comparison between identified and analytical mode shapes was also performed graphically (Fig. 15), and this reveals that, similarly to the previous experimental case study, also for this second case study, it is more difficult to rely on the high-order mode shapes to perform the classification. As shown in Fig. 15, it seems to be difficult to associate the modal vector for the 2nd and 3rd modes to one model or to the other. The first mode, on the contrary, provides a much clearer indication, and from the observations of its mode shape and the related values of NA1 and NA2, it can be inferred that the structure has a behavior that is more similar to the GA beam model. This deduction is also confirmed by the ratios of the natural frequencies, which are provided in Table 7. As shown in the table, the frequency ratios of the 5-story building match well with the ratios evaluated for the shear-deflecting cantilever beam.

After the executed structure-type classification, the case study was analyzed through the flexibility deflection-based method for damage detection that uses the interstory drifts as damage-sensitive features, as shown in Sect. 2. The modal flexibility matrices were assembled using the identified

**Table 5** Identified natural frequencies of the 5-story building in the different states

State	Natural frequency $f_i$ [Hz] (% variation w.r.t. baseline state C0)		
	1st mode	2nd mode	3rd mode
C0 <sup>a</sup>	1.57	5.89	10.80
C1	1.42 (– 9.6)	5.27 (– 10.5)	10.55 (– 2.3)
C2	1.27 (– 19.1)	4.99 (– 15.3)	8.13 (– 24.7)

<sup>a</sup>Mean values of natural frequencies (for all considered baseline data)

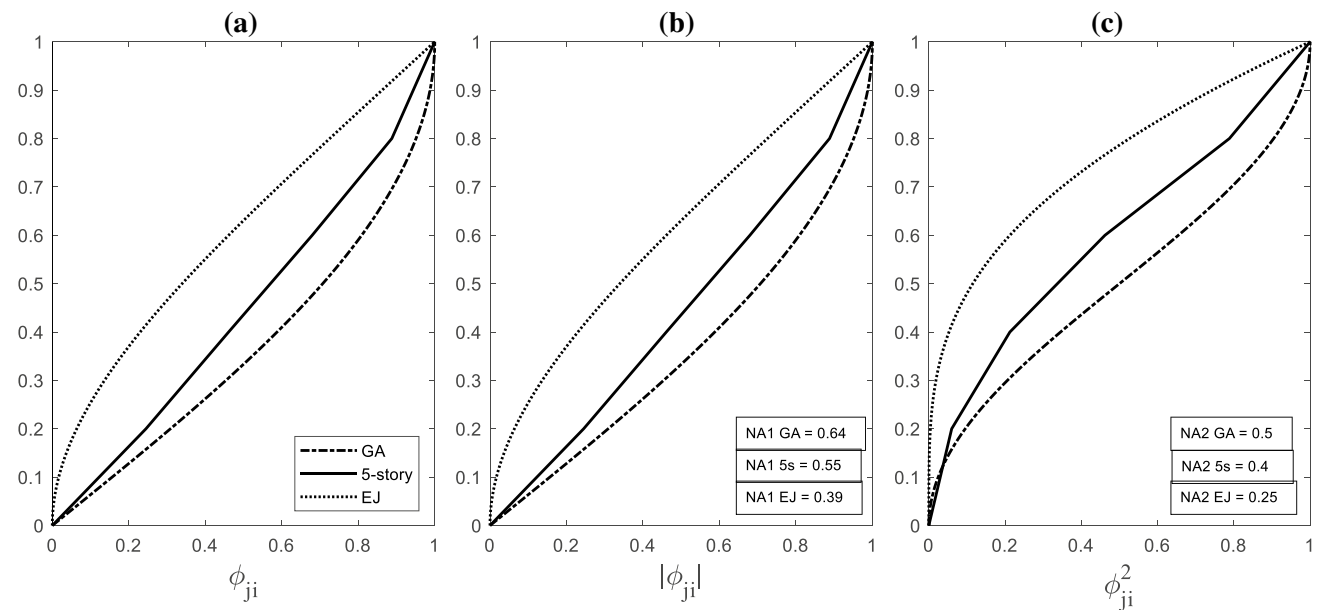


**Fig. 14** Mode shape (a) and normalized areas (b, c) for the first mode of the 5-story building (results compared with the analytical models)

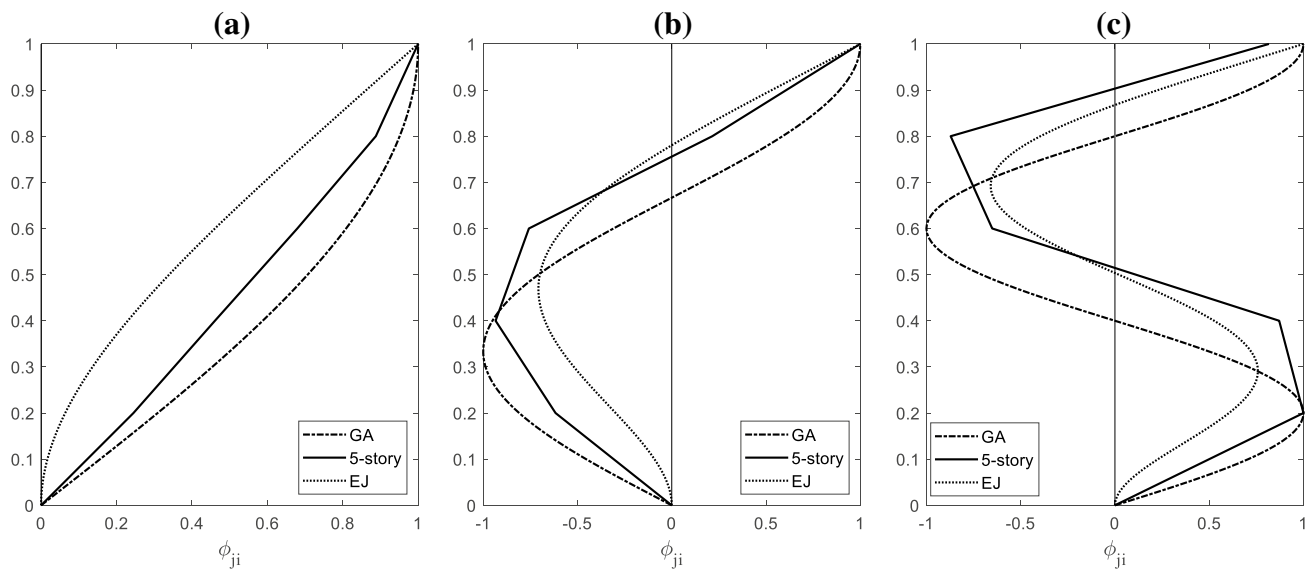


**Fig. 15** Mode shapes for the 5-story building and comparison with the analytical models: **a** 1st mode; **b** 2nd mode; **c** 3rd mode

**Table 7** Ratios of the natural frequencies for the 5-story building and comparison with the analytical models

State C0	Natural frequency ratios	
	$f_2/f_1$	$f_3/f_1$
Experimental case—5 story building	3.75	6.87
Analytical model—EJ cantilever beam	6.32	17.54
Analytical model—GA cantilever beam	3	5

modal parameters, and, similarly to the previous case study, the normalization of the mode shapes for the flexibility estimation was performed using a diagonal proportional mass matrix that was estimated using the information available about the structure. The deflections were then determined by applying inspection loads that are uniform loads with unitary values at all the floor levels.

The modal flexibility-based deflections and the interstory drifts of the 5-story building are shown in Figs. 16 and 17. In Fig. 16, the inspected state C1 is compared with the baseline state C0 (both states tested with 3%g RMS white noise excitation), while in Fig. 17, the configuration C2 is considered in the inspection phase and compared with the reference state C0 (both configurations tested with 3.5%g RMS white noise excitation). The trends of the experimentally identified deflections and the related interstory drifts are in agreement with those of the corresponding quantities expected for a frame structure with a story stiffness that is substantially uniform along with the height and that is loaded by uniform loads. The values of the interstory drifts for the baseline structure tend to increase from the upper to

the lower stories, as expected. Moreover, it can be observed in Figs. 16, 17 that the values of the displacements related to the inspected states are higher than the corresponding values related to the baseline state. This is evident in the comparison between states C0–C1 (Fig. 16), and it is even more evident in the comparison between states C0–C2 (Fig. 17). The observed increments in the values of the displacements indicate that structural modifications which can be associated with damage have occurred in the inspected states. This is also confirmed by the values of the natural frequencies for the different states (Table 5). All the frequencies related to the damaged states (C1 and C2) are lower than the frequencies of the baseline state (C0), as expected. Moreover, the frequencies of configuration C2 are lower than the frequencies of configuration C1. These two configurations were in fact tested one after the other, with configuration C2 that has been exposed to a higher number of and more severe earthquakes.

Figure 18 shows the results of the damage localization both for configurations C1 and C2: in Fig. 18a, the damage-induced interstory drifts are provided (i.e., the difference between the interstory drift in the damaged state and the interstory drift in the baseline state), while Fig. 18b shows the values of the z-index based on interstory drift (Eq. 9). It is evident from Fig. 18b that, for both configurations C1 and C2, the z-index overpasses the threshold at the 2nd story, which, according to the observations in [36, 39], is one of the stories that were affected by more damage. It is worth noting that the z-index takes into account both the variations in the interstory drifts and the statistical variability related to the baseline state, and in Fig. 18b, the values of the z-index at first story are below

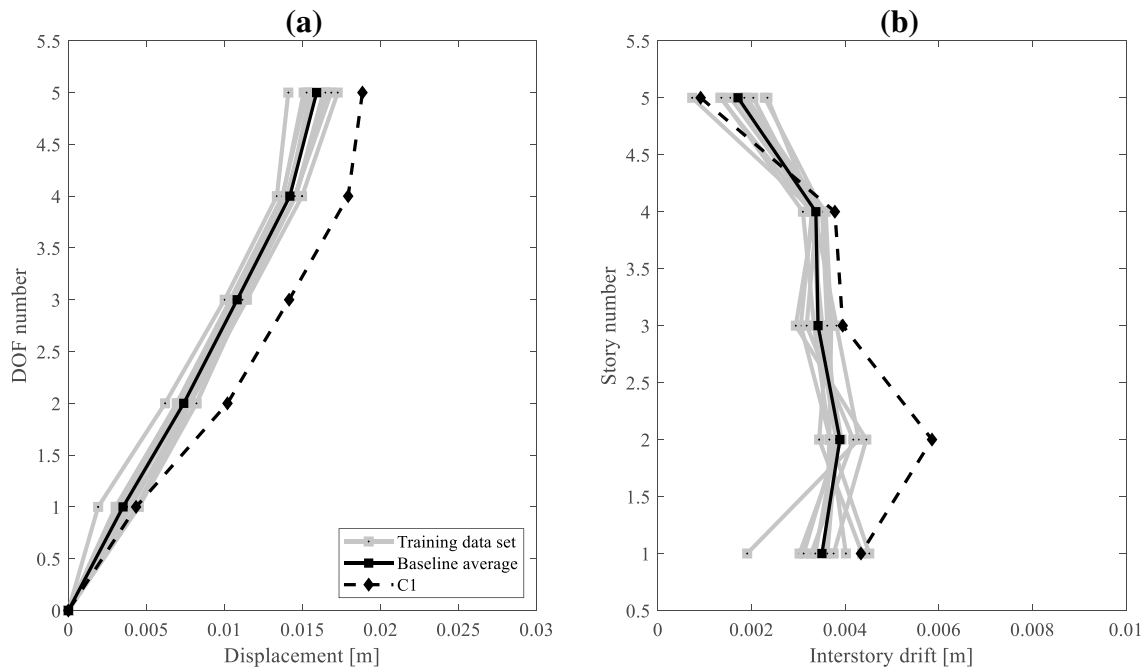


**Fig. 16** Modal flexibility-based deflections of the 5-story building (configurations C0–C1): **a** displacements; **b** interstory drifts

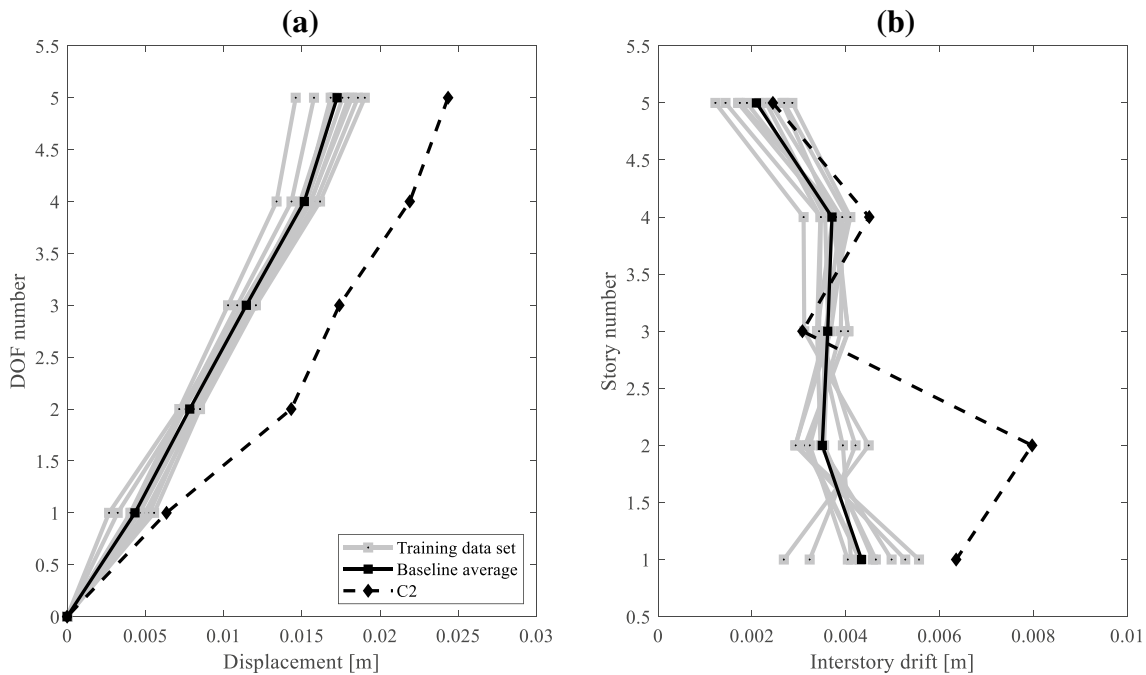


**Fig. 17** Modal flexibility-based deflections of the 5-story building (configurations C0–C2): **a** displacements; **b** interstory drifts

the threshold similarly to the corresponding values related to the upper stories. A more careful examination of the results through the analysis of the damage-induced interstory drifts (Fig. 18a), however, reveals that the condition of the first story should not be considered as identical to

that of the upper stories. In Fig. 18a, it is in fact evident that the damage-induced interstory drifts at the lower stories (i.e., first and second stories) tend to be higher than the damage-induced interstory drifts at the upper stories, and this is consistent with the actual damage that has been

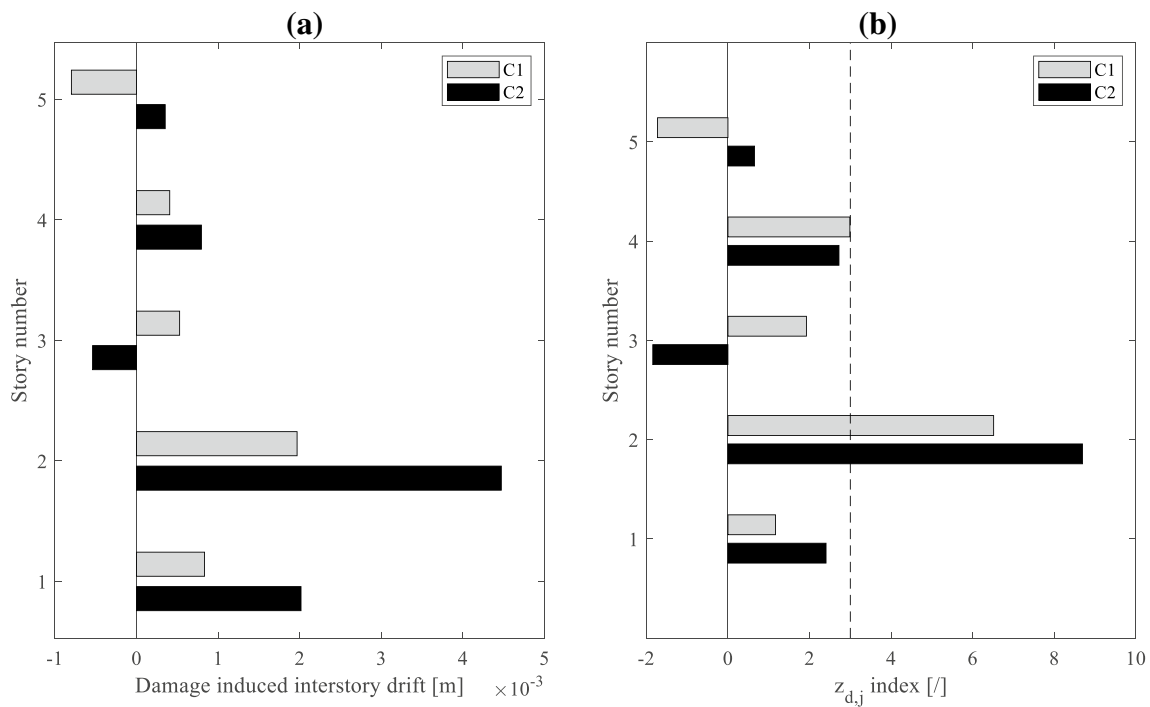


**Fig. 18** Damage detection and localization for the 5-story building: **a** damage-induced interstory drift; **b**  $z$ -index based on interstory drifts (where the dashed line represents the threshold value)

observed on the structure during the experimental tests. The performed analyses revealed that, due to the characteristics of the recorded signals in the baseline state, the lower DOFs' components of the identified mode shapes are affected by more uncertainties. For the evaluation of the cross-correlation functions used in the NExT-ERA algorithm, the reference channel was selected as the channel located at the top floor level of the structure, according to the indications provided in [41], and this could also have an influence on the outcomes of the modal identification process. Uncertainties on the mode shapes are in turn reflected in the modal flexibility-based interstory drifts. As shown in Figs. 16b and 17b, the variability on the drifts for the baseline state is more pronounced especially at the first story, and this could be one of the main reasons for which the damage at first story of the selected case study tends to be identifiable only using the damage-induced interstory drifts (Fig. 18a) and not using the  $z$ -index (Fig. 18b). This result obtained for the selected case study suggests that when an alert is provided by the algorithm (such as the case of the  $z$ -index overpassing the threshold at the second story in Fig. 18b), it is generally always useful to check the results related to the intermediate steps of the damage detection process, to have more insight into the characteristics of the observed damaged condition.

The method based on the evaluation of the variations in the interstory drifts described in Sect. 2 is applied herein

only for damage detection and localization purposes, and not for damage quantification purposes (similarly to the method based on the flexibility deflection-based curvature applied for the first case study). Despite this, referring to Fig. 18, it is interesting to note that the quantities obtained at the damaged stories for configuration C2 (both the  $z$ -index and the damage-induced interstory drift) tend to be higher than the corresponding quantities related to configuration C1. This is clearly correlated with the fact that, as explained in [36, 39], configuration C2 has been exposed to more severe earthquakes and has been affected by more severe damage.

## 5 Conclusions

The present study has addressed the problem of classifying the typology of building structures using vibration data only and in the framework of the flexibility deflection-based methods for damage detection and localization. The classification is, in fact, a crucial operation to be performed for selecting the most appropriate algorithms and damage-sensitive features. The objective of the study was also to test the applicability of the considered methods on full-scale reinforced concrete structures that have experienced earthquake-induced damage. First, a summary of the considered methods for damage detection in building structures was presented. Then, different criteria were presented for

structure-type classification using two proposed indices, NA1 and NA2, evaluated for each experimentally derived mode shape of the structure. The proposed criteria have been derived using the theory of continuous cantilever beam models (i.e., bending-moment-deflecting beam and shear-deflecting beam) and are thought to be complementary to the more traditional approach based on the estimation of the ratios of identified natural frequencies. The values provided by the proposed indices NA1 and NA2 depend on the shape of the modal vectors, and, for each of the considered reference models, these values are constant (or at least very similar) for all the different modes. In the index NA1, the modulus of each mode shape component is used, while the index NA2 adopts the squared value of each component. A parametric analysis was also performed to simulate the discretization that the mode shapes can have when are identified from real experimental tests and to study the behavior of the proposed indices in different scenarios with mode shapes defined by an increasing number of points. The analysis has shown that the indices for the low-order modes converge more rapidly to the reference values than the indices related to the high-order modes. Moreover, different results for the two proposed indices NA1 and NA2 were obtained in the parametric analysis, suggesting that, from the theoretical point of view, the index NA2 might be more effective than the index NA1, especially when considering the high-order modes.

The criteria for structure-type classification and the damage detection methods have been applied using the vibration data of two reinforced concrete building structures tested on the University of California, San Diego-Network for Earthquake Engineering Simulation (UCSD-NEES) large outdoor unidirectional shake table. For these experimental case studies, the proposed criteria and indices NA1 and NA2 have proven effective for classifying the structural typology, especially using the first mode shape. This resulted in classification outcomes that agreed with those derived from the analysis of the natural frequency ratios. Through the classification criteria and the data analysis, it was possible to show that the first case study (i.e., 7-story building slice) can be modeled as a bending-moment-deflecting cantilever beam. For this case study, the flexibility deflection-based curvature was thus considered as the damage-sensitive feature. On the contrary, the analyses revealed that the 5-story building has a behavior more similar to that of a shear-deflecting cantilever beam model. For this second case study, the damage localization was thus performed by analyzing the interstory drifts computed from the deflections. Overall, the damage detection analyses have demonstrated the applicability of the considered vibration-based methods to full-scale structures that have experienced earthquake-induced damage, providing localization results consistent with the positions of the actual damage observed in the structures during the experimental tests.

**Acknowledgements** The use of the data of the experimental tests performed on the 7-story RC wall building and on the 5-story RC frame building using the UCSD-NEES shake table (Englekirk Structural Research Center, San Diego, USA) is gratefully acknowledged.

**Author contributions** Conceptualization: GB, SQ, LL, and PPD; investigation: GB; methodology: GB and SQ; software: GB; supervision: LL and PPD; visualization: GB and SQ; writing—original draft: GB and SQ; writing—review and editing: LL and PPD.

**Funding** Open access funding provided by Alma Mater Studiorum - Università di Bologna within the CRUI-CARE Agreement. For conducting this study, no funding was received outside of the primary affiliations of the authors.

**Availability of data** The data of the experimental tests performed on the 7-story RC wall building and on the 5-story RC frame building using the UCSD-NEES shake table (Englekirk Structural Research Center, San Diego, USA) were used in this paper. The data of these tests are openly available in DesignSafe at <https://doi.org/10.4231/D35T3G04T> (7-story building) and <https://doi.org/10.4231/D38W38349> (5-story building).

## Declarations

**Conflict of interests** The authors declare that they have no known competing financial interests or personal relationships that could have appeared to influence the work reported in this paper.

**Open Access** This article is licensed under a Creative Commons Attribution 4.0 International License, which permits use, sharing, adaptation, distribution and reproduction in any medium or format, as long as you give appropriate credit to the original author(s) and the source, provide a link to the Creative Commons licence, and indicate if changes were made. The images or other third party material in this article are included in the article's Creative Commons licence, unless indicated otherwise in a credit line to the material. If material is not included in the article's Creative Commons licence and your intended use is not permitted by statutory regulation or exceeds the permitted use, you will need to obtain permission directly from the copyright holder. To view a copy of this licence, visit <http://creativecommons.org/licenses/by/4.0/>.

## References

1. Farrar CR, Worden K (2013) Structural health monitoring: a machine learning perspective, 1st edn. Wiley, Chichester
2. Rainieri C, Fabbrocino G (2014) Operational modal analysis of civil engineering structures. Springer, New York
3. Brincker R, Ventura CE (2015) Introduction to operational modal analysis, 1st edn. Wiley, Chichester
4. Rainieri C, Fabbrocino G (2010) Automated output-only dynamic identification of civil engineering structures. *Mech Syst Signal Process* 24(3):678–695. <https://doi.org/10.1016/j.ymssp.2009.10.003>
5. Pandey AK, Biswas M (1994) Damage detection in structures using changes in flexibility. *J Sound Vib* 169(1):3–17. <https://doi.org/10.1006/jsvi.1994.1002>
6. Bernal D (2001) A subspace approach for the localization of damage in stochastic systems. In: Chang FK (ed) Structural health monitoring: the demand and challenges—proceedings of the 3rd international workshop in structural health monitoring, pp 899–908. CRC Press, Boca Raton



7. Gao Y, Spencer BF Jr, Bernal D (2007) Experimental verification of the flexibility-based damage locating vector method. *J Eng Mech* 133(10):1043–1049. [https://doi.org/10.1061/\(ASCE\)0733-9399\(2007\)133:10\(1043\)](https://doi.org/10.1061/(ASCE)0733-9399(2007)133:10(1043))
8. Duan Z, Yan G, Ou J, Spencer BF (2005) Damage localization in ambient vibration by constructing proportional flexibility matrix. *J Sound Vib* 284:455–466. <https://doi.org/10.1016/j.jsv.2004.06.046>
9. Duan Z, Yan G, Ou J, Spencer BF (2007) Damage detection in ambient vibration using proportional flexibility matrix with incomplete measured DOFs. *Struct Control Health Monit* 14(2):186–196. <https://doi.org/10.1002/stc.149>
10. Zhang Z, Aktan AE (1998) Application of modal flexibility and its derivatives in structural identification. *Res Nondestr Eval* 10(1):43–61. <https://doi.org/10.1007/PL00003899>
11. Koo KY, Sung SH, Park JW, Jung HJ (2010) Damage detection of shear buildings using deflections obtained by modal flexibility. *Smart Mater Struct* 19(11):115026. <https://doi.org/10.1088/0964-1726/19/11/115026>
12. Bernagozzi G, Ventura CE, Allahdadian S, Kaya Y, Landi L, Diotallevi PP (2020) Output-only damage diagnosis for plan-symmetric buildings with asymmetric damage using modal flexibility-based deflections. *Eng Struct* 207:110015. <https://doi.org/10.1016/j.engstruct.2019.110015>
13. Bernagozzi G, Mukhopadhyay S, Betti R, Landi L, Diotallevi PP (2018) Output-only damage detection in buildings using proportional modal flexibility-based deflections in unknown mass scenarios. *Eng Struct* 167:549–566. <https://doi.org/10.1016/j.engstruct.2018.04.036>
14. Koo KY, Sung SH, Jung HJ (2011) Damage quantification of shear buildings using deflections obtained by modal flexibility. *Smart Mater Struct* 20:045010. <https://doi.org/10.1088/0964-1726/20/4/045010>
15. Catbas FN, Gul M, Burkett JL (2008) Damage assessment using flexibility and flexibility-based curvature for structural health monitoring. *Smart Mater Struct* 17(1):015024. <https://doi.org/10.1088/0964-1726/17/01/015024>
16. Koo KY, Lee JJ, Yun CB, Kim JT (2008) Damage detection in beam-like structures using deflections obtained by modal flexibility matrices. *Smart Struct Syst* 4(5):605–628. <https://doi.org/10.12989/sss.2008.4.5.605>
17. Sung SH, Jung HJ, Jung HY (2013) Damage detection for beam-like structures using the normalized curvature of a uniform load surface. *J Sound Vib* 332(6):1501–1519. <https://doi.org/10.1016/j.jsv.2012.11.016>
18. Sung SH, Koo KY, Jung HJ (2014) Modal flexibility-based damage detection of cantilever beam-type structures using baseline modification. *J Sound Vib* 333(18):4123–4138. <https://doi.org/10.1016/j.jsv.2014.04.056>
19. Le NT, Nguyen A, Thambiratnam DP, Chan THT, Khuc T (2020) Locating and quantifying damage in beam-like structures using modal flexibility-based deflection changes. *Int J Struct Stab Dyn* 20(10):2042008. <https://doi.org/10.1142/S0219455420420080>
20. Catbas FN, Brown DL, Aktan AE (2006) Use of modal flexibility for damage detection and condition assessment: case studies and demonstrations on large structures. *J Struct Eng* 132(11):1699–1712. [https://doi.org/10.1061/\(ASCE\)0733-9445\(2006\)132:11\(1699\)](https://doi.org/10.1061/(ASCE)0733-9445(2006)132:11(1699))
21. Sung SH, Koo KY, Jung HY, Jung HJ (2012) Damage-induced deflection approach for damage localization and quantification of shear buildings: validation on a full-scale shear building. *Smart Mater Struct* 21(11):115013. <https://doi.org/10.1088/0964-1726/21/11/115013>
22. Le NT, Thambiratnam DP, Nguyen A, Chan THT (2019) A new method for locating and quantifying damage in beams from static deflection changes. *Eng Struct* 180:779–792. <https://doi.org/10.1016/j.engstruct.2018.11.071>
23. Quqa S, Landi L, Diotallevi PP (2018) On the use of singular vectors for the flexibility-based damage detection under the assumption of unknown structural masses. *Shock Vib*. <https://doi.org/10.1155/2018/9837694>
24. Pandey AK, Biswas M, Samman MM (1991) Damage detection from changes in curvature mode shapes. *J Sound Vib* 145(2):321–332. [https://doi.org/10.1016/0022-460X\(91\)90595-B](https://doi.org/10.1016/0022-460X(91)90595-B)
25. Giordano PF, Limongelli MP (2020) Response-based time-invariant methods for damage localization on a concrete bridge. *Struct Concr* 21(4):1254–1271. <https://doi.org/10.1002/suco.202000013>
26. Clough RW, Penzien J (1995) Dynamics of structures. Computers & Structures Inc, London
27. Chopra AK (1995) Dynamics of structures: theory and applications to earthquake engineering. Prentice Hall, Hoboken
28. Bernal D (2002) Load vectors for damage localization. *J Eng Mech* 128(1):7–14. [https://doi.org/10.1061/\(ASCE\)0733-9399\(2002\)128:1\(7\)](https://doi.org/10.1061/(ASCE)0733-9399(2002)128:1(7))
29. Panagiotou M, Restrepo JI, Conte JP (2007) Shake table test of a 7 story full scale reinforced concrete structural wall building slice—phase I: rectangular wall section. In: Report No SSRP-07/07, University of California, San Diego
30. Moaveni B, He X, Conte JP, Restrepo JI (2010) Damage identification study of a seven-story full-scale building slice tested on the UCSD-NEES shake table. *Struct Saf* 32(5):347–356. <https://doi.org/10.1016/j.strusafe.2010.03.006>
31. Moaveni B, He X, Conte JP, Restrepo JI, Panagiotou M (2011) System identification study of a 7-story full-scale building slice tested on the UCSD-NEES shake table. *J Struct Eng (ASCE)* 137(6):705–717. [https://doi.org/10.1061/\(ASCE\)ST.1943-541X.0000300](https://doi.org/10.1061/(ASCE)ST.1943-541X.0000300)
32. Panagiotou M, Restrepo J, Conte J (2006) Shake table test of 7-story RC bearing wall building. *DesignSafe-CI*. <https://doi.org/10.4231/D35T3G04T>
33. Juang JN, Pappa RS (1985) An eigensystem realization algorithm for modal parameter identification and model reduction. *J Guid Control Dyn* 8(5):620–627. <https://doi.org/10.2514/3.20031>
34. James GH III, Carne TG, Lauffer JP (1995) The natural excitation technique (NExT) for modal parameter extraction from operating structures. *Int J Anal Exp Modal Anal* 10(4):260–277
35. Chen MC, Pantoli E, Wang X, Astroza R, Ebrahimian H, Mintz S, Hutchinson T, Conte J, Restrepo J, Meacham B, Kim J, Park H (2013) BNCS Report #1: full-scale structural and nonstructural building system performance during earthquakes and post-earthquake fire—specimen design, construction and test protocol, Structural Systems Research Project Report Series, SSRP 13/9, University of California San Diego, La Jolla, CA
36. Pantoli E, Chen M, Wang X, Astroza R, Mintz S, Ebrahimian H, Hutchinson T, Conte J, Restrepo JI, Kim J, Park H, Meacham BJ, Kim J, Park H (2013) BNCS Report #2: full-scale structural and nonstructural building system performance during earthquakes and post-earthquake fire—test results, Structural Systems Research Project Report Series, SSRP 13/10, University of California San Diego, La Jolla, CA
37. Pantoli E, Chen M, Hutchinson T, Restrepo JI (2013) BNCS Report #3: full-scale structural and nonstructural building system performance during earthquakes and post-earthquake fire—camera and analog sensor details, Structural Systems Research

- Project Report Series, SSRP 13/11. University of California San Diego, La Jolla, CA
38. Chen MC, Pantoli E, Wang X, Hutchinson T, Restrepo J (2013) BNCS Report #4: full-scale structural and nonstructural building system performance during earthquakes and post-earthquake fire—construction details and technical specifications of specific subsystems, Structural Systems Research Project Report Series, SSRP 13/12, University of California San Diego, La Jolla, CA
  39. Astroza R, Ebrahimian H, Conte JP, Restrepo JI, Hutchinson TC (2016) System identification of a full-scale five-story reinforced concrete building tested on the NEES-UCSD shake table. *Struct Control Health Monit* 23:535–559. <https://doi.org/10.1002/stc.1778>
  40. Hutchinson T, Restrepo J, Conte J, Pantoli E, Chen M, Wang X, Astroza R, Ebrahimian H (2012) Shake table testing of a five-story building outfitted with NCSs (BNCS project). DesignSafe-CI. <https://doi.org/10.4231/D38W38349>
  41. Caicedo JM (2011) Practical guidelines for the natural excitation technique (NExT) and the eigensystem realization algorithm (ERA) for modal identification using ambient vibration. *Exp Tech* 35(4):52–58. <https://doi.org/10.1111/j.1747-1567.2010.00643.x>

**Publisher's Note** Springer Nature remains neutral with regard to jurisdictional claims in published maps and institutional affiliations.